Multibody Simulation of a simple Gear Transmission System using Ansys Motion drive train Toolkit

Bryan Pacheco

November 15, 2022

Contents

1 Introduction

As a milestone to the implementation of a gear testing bench a previous study on a dedicated multibody (MBD) simulation environment is performed. In this fashion, an initial goal is to gain reliable predictions of the dynamic behaviour of one testing set up under any desired load condition while considering relevant geometry modifications. The first approach to this consists in the simulation of the gear dynamics of a simple transmission system that will allow the comparison of the retrieved results with a straight-forward analytical method, thus allowing the validation of the software reliability and setting up a basis for a further investigation on the dynamics of the system.

The present short report serves primarily as a summary to these first findings and presents a discussion based on the current knowledge about gear mesh. Since it was also possible to analyse the periodic nature of the transmission through the use of Fast Fourier Transformations (FFT), an insight on the expected dynamics of the system is also provided.

2 State of Science and Technology

2.1 Theoretical Framework

The technical knowledge regarding the analysis of a rotating system such as a drive train can be quite broad due to the variety of gears and possible configurations that can be employed. For this reason, the present theoretical framework is limited to the parallel spur gear couplings and mainly focused in the idler gear set type (refer to chapter 5.1), since it corresponds to the system to be studied in Ansys Motion.

The physical behaviour of any gear set can be classified into the field of rotational mechanics, which can be roughly described as a collection of bodies (gears) that rotate based on certain conditions and constraints inherent to the system. Depending on the level of fidelity of the mathematical model, different analysis can be performed [1]. In the context of this report, the approach is divided into the gear kinematics and dynamics, respectively.

2.1.1 Gear Kinematics

The kinematics of rotationally connected bodies consists on a very simplified representation of the system because it is based on the model of rigid elements. Nevertheless, it is the most fundamental to assessing the basic operation and performance of a drive train, requiring the least fidelity to mathematically model and solve. [1] Therefore, it is a logical first step for understanding the physical nature of any gear set.

For this type of study, an initial three-dimensional representation is normally the case (see Figure 1). As long as a congruent axis of rotation is assumed for each rotating body and under consideration that the rotational couplings between bodies affect only the motion about each axis of rotation, the study

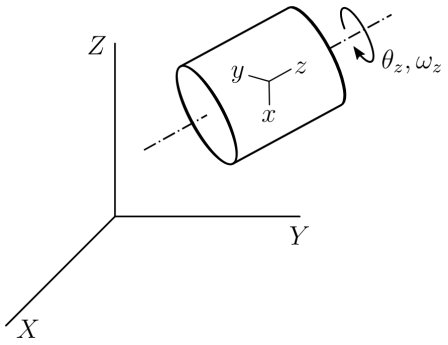

Figure 1: Three-dimensional representation of a rotational rigid body in cartesian space. Here the axis of rotation is set in the z-direction according to the body coordinate system. [1]

of any system of arbitrarily oriented bodies can be reduced to the analysis of one single degree-of-freedom (DOF). Specifically, kinematics is firstly interested in the rate of change of the DOF, θ (angular displacement), about the axis of rotation: [1].

$$\vec{\omega} = \frac{\mathrm{d}\vec{\theta}}{\mathrm{d}t} \tag{1}$$

Where ω is known as the angular velocity of the body. Two gears form a gear pair when they are rotationally coupled by the meshing gear teeth (tooth engagement is the mean of power transmission). In this case, each gear body is modeled with a single degree of freedom and two variables are needed to define the kinematics of the system: ω_1, ω_2. In a drive train with more than two gears in parallel, it is said that multiple gear pairs are rotationally coupled. For the idler gear set (Figure 2), a total number of two gear pairs is considered and three variables describe the kinematics of the system: ω_1, ω_2, ω_3. [1]

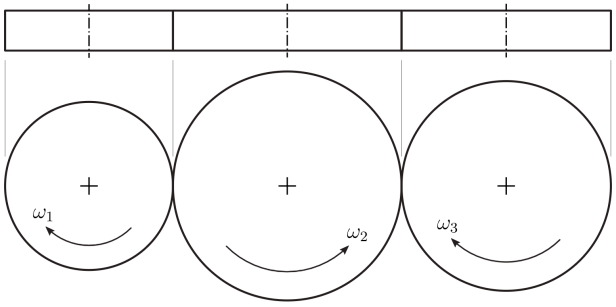

Figure 2: Kinematic diagram of an idler gear set (top and front views). [1]

In order to solve for the kinematics of this assembly, a system with a number

of equations equal to the quantity of unknown variables must be formulated. The equations have to be a function of those variables. Based on the fact that the tangential speed at each meshing point is the same for both gears that form a coupled pair, the following relation can be defined for the input-idler gear pair at the contact point:

$$|\vec{v_{t1}}| = |\vec{v_{t2}}| \tag{2}$$

$$|\vec{\omega_1}|r_1 = |\vec{\omega_2}|r_2 \tag{3}$$

$$\frac{|\vec{\omega_1}|}{|\vec{\omega_2}|} = \frac{r_2}{r_1} \tag{4}$$

With the introduction of the gear module m, as the ratio between the pitch diameter d_p and the number of teeth z, the angular velocity can now be expressed in terms of the transmission ratio, i:

$$\frac{r_2}{r_1} = \frac{d_{p2}}{d_{p1}} = \frac{mz_2}{mz_1} \tag{5}$$

$$\therefore i_{12} = \frac{z_2}{z_1} = \frac{|\vec{\omega_1}|}{|\vec{\omega_2}|} \tag{6}$$

By knowing that coupled gears in an external gear mesh rotate in opposite directions and that a single component of each angular velocity vector is non-zero, the classical form of a linear equation can be written as: [1]

$$\omega_1 + i_{12}\omega_2 = 0 \tag{7}$$

In a similar way, a linear equation for the idler-output gear pair is formulated:

$$\omega_2 + i_{23}\omega_3 = 0 \tag{8}$$

The full definition of the kinematics comes from the imposition of a constraint on the system. Normally this occurs through a specified constant input speed Ω_1 that defines the last required equation:

$$\omega_1 = \Omega_1 \tag{9}$$

Finally, the system of equations for kinematics of a parallel idler gear set is assembled in matrix form as: [1]

$$\begin{bmatrix} 1 & 0 & 0 \\ 1 & i_{12} & 0 \\ 0 & 1 & i_{23} \end{bmatrix} \begin{bmatrix} \omega_1 \\ \omega_2 \\ \omega_3 \end{bmatrix} = \begin{bmatrix} \Omega_1 \\ 0 \\ 0 \end{bmatrix} \tag{10}$$

Usually the input speed constraint is a known parameter of the system, which explains why the first analytical solutions account for the angular velocity as the variable that represents the DOF of each gear. Despite this, the change over

time of the displacement and acceleration (both linear and angular) can also be of particular interest in a kinematic analysis. For that purpose, any desired function can be easily derived by means of the following relations:

$$|\vec{s}| = |\vec{\theta}|r \qquad\qquad |\vec{a}| = |\vec{\alpha}|r \tag{11}$$

$$\vec{\theta} = \int \vec{\omega} \mathrm{d}t \qquad\qquad \vec{\alpha} = \frac{\mathrm{d}\vec{\omega}}{\mathrm{d}t} \tag{12}$$

Throughout the previous formulations all angular variables were referred to the movement around the gear's rotational axis. Assuming the body coordinate system of Figure 1, a better notation should be θ_z, ω_z and α_z of the respective gears. For the translational variables it is important to notice that the values obtained correspond to a magnitude. That means that its value does not refer to a single axis and as such, it can still be broken down into its x, y and z components. In practice, sensors can be placed in a gear system to measure linear variations in the three directions, making it important to analyse them individually as well. Because the system is constrained to rotate about a particular axis (i.e. z), the average speed of any off-axis rotations must be zero in a kinematic analysis. The remaining components (x and y) describe a periodic oscillatory movement. If the gear's angular velocity is kept constant, the magnitude of the linear velocity is constant as well. Opposite to this, the components of the linear velocity change over time as they describe a simple harmonic motion (SHM). This occurs because in the x and y directions only the axis-projections of the uniform circular motion are described.

Since the SHM has a constant angular frequency (equal to the angular velocity of the body), the linear velocity functions in each axis are practically the same, only being out of phase with which other by 90 degrees. For a constant angular frequency study, it should be enough to analyse the motion in just one direction. An easier way to understand this motion is by looking at the displacement function.

Figure 3 illustrates how the vectorial components of the displacement change as the circular body undergoes a SHM. By taking the y direction as a reference, the displacement function of the point fixed in the circumference of rotating body can be modelled with the following equation:

$$y(t) = r\cos(\omega t) \tag{13}$$

Where $y(t)$ is the vertical position of the marker as it changes over the time t, with the angular frequency ω. Moreover, by obtaining the first and second derivatives of this function it is possible to also get the expressions for linear velocity and acceleration, respectively:

$$v_y(t) = \frac{\mathrm{d}y(t)}{\mathrm{d}t} = -\omega r\sin(\omega t) \tag{14}$$

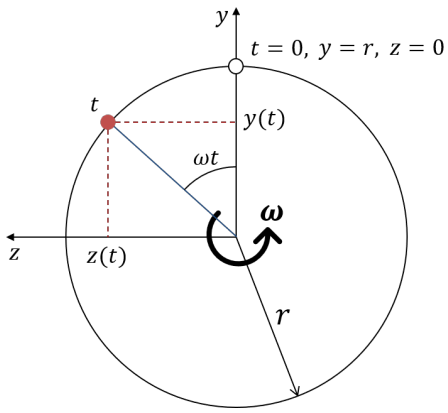

Figure 3: Vectorial representation of the circular displacement of a fixed point in the circumference of a rotating body in simple harmonic motion. Reference body, coordinate system and marker based on the gear models described in Figures 5 and 9.

$$a_y(t) = \frac{\mathrm{d}^2 y(t)}{\mathrm{d}t^2} = -\omega^2 r \cos(\omega t) \tag{15}$$

The same procedure is followed to get the equations in the z direction:

$$z(t) = r \sin(\omega t) \tag{16}$$

$$v_z(t) = \omega r \cos(\omega t) \tag{17}$$

$$a_z(t) = -\omega^2 r \sin(\omega t) \tag{18}$$

2.1.2 Gear Multibody Dynamics

Unlike kinematics, the dynamic analysis does not rely exclusively on the geometrical information of the system. Here the consideration of masses, inertias, forces and moments plays a major role when modelling the drive train. Furthermore, a gearbox is a system composed of different bodies such as gears, shafts, bearings and housing, and the interaction between all of them is important to properly model the dynamic behaviour of the whole assembly. For that reason, referring to gear dynamics always involve the consideration of multibody dynamics. From an analytical point of view, the topic can be really complex, so it will not be fully discussed, as it is not within the scope of this work. The main aspects regarding MBD calculations are assumed to be performed by the software (sections 2.1.3 and 2.1.5) and only key concepts regarding the gear-gear interaction are the focus of this subchapter, since it is essentially what is being modelled and simulated (see chapter 5.1).

Depending on the conditions imposed to the system, a dynamic response can be distinguished between a steady state (linearized frequency domain) and a transient (linear and non-linear time domain) one. [1] To have reliable data of those responses is a critical step when analysing rotating machinery because they have direct influence on the noise and vibration outcome, which lately defines the overall performance of the machine and can help to accurately predict failures and maintenance needs.

Relevant literature: [2] [3] [4] [5] [6] [7] [8] [9] [10] [11] [12] [13] [14] [15] [16] [17] [18]

2.1.3 Multibody simulation

Topics to be discussed:

2.1.4 Gear meshing

A gear pair when subjected to loading, experiences teeth deformation in the form of contact and bending, the resistance to which is characterized by the mesh stiffness. It depends on the geometric and material properties on the gear system and is important element of internal excitation in a dynamic system. The number of teeth in contact varies through the mesh cycle, which results in a time-dependent variation in this mesh stiffness. As compared to the spur gears, helical gears have a helix angle which guides the teeth incline[19]. The helix angle facilitates the gradual meshing of gear teeth, which reduces load fluctuations. This results in a smoother variation in teeth contact, leading to a lower mesh stiffness fluctuation. In contrast, a spur gear pair displays more pronounced fluctuations due to instantaneous meshing[20].

- Transmission error: Gear transmission error is the difference in torsional vibration of two gears in mesh, to give the representation of linear motion along the line of action. Some factors affecting the transmission error are tooth geometry errors (manufacturing imperfection or wear), elastic deformation and misalignment due to geometric errors. The transmission error has the following types- The static transmission error (STE), which includes the elastic deformation of teeth and is load dependent, and the dynamic transmission error (DTE), including inertial and stiffness effects, hence being both speed and load dependent[21]. Transmission error can be measured by phase demodulation of pulse signals from shaft encoders on the free ends of the shafts on which the gears are mounted[22]. Another metric used for distinguishing errors in gear transmission is the peak-to-peak transmission error (PPTE), which is defined as the difference of maximum and minimum STE. It provides a method to a single value for describing the STE [23]. Transmission errors in gear systems are caused by manufacturing and assembly imperfections and elastic deflections of gear teeth, shafts, bearings, and housing.

- Vibration analysis: Natural frequencies and vibration modes are calculated by the free vibration analysis, which is essential for the investigation of the gear dynamics phenomena. The vibration properties are also important for the further analysis of eigen sensitivity to design parameters and parametric instabilities from mesh stiffness variations. The study of system frequency aids the design process, so as to avoid frequency resonance. The natural modes of vibration are inherent to a dynamic system and are defined completely by the physical properties and their spatial distributions.The modal frequencies can determine the mode shape or pole location[24]. The vibration issues result in undesirable noise in the system. Gear whine is caused by meshing impacts or tooth parametric quality variations. Rattle is a broadband frequency caused by the meshing of the transmission loose gears and is found as a result of two factors: torsional vibration excitation level at the transmission input shaft and the rattle sensitivity of the transmission at that excitation level[25]. Vibration analysis plays a critical role in in understanding the rattle and whine noises present in the a gear system.

- Gear defects/faults: Vibration analysis plays an important role in early fault detection in transmission systems. The vibration signature can provide a variety of information on many structures such as gear meshing frequencies, structural resonances and faults. Vibration analysis techniques such as the residual signal and demodulation techniques are able to localize the damaged tooth. The gear vibration spectra usually show sidebands of meshing frequency and its harmonics. Changes in the number and amplitude of sidebands normally indicate a deteriorating condition[26].

2.1.5 Ansys Motion Drive train Toolkit

Ansys Motion Drive train is a specialized toolkit for analysing noise, vibration and harshness (NVH) characteristics of drivetrain systems including gears, bearings, shafts and housings. System analysis in time domain based on dynamic analysis. It can conduct analyses from the initial design concept through to detailed production models. Waterfall colour maps and order tracking data can be produced in the same manner as in a real-world test environment to allow easy comparison of simulation and reality.Gear whine and rattle characteristics can be analysed. Gear profile can be modified after analysing the gear results.
Advantages:

- Supports various features to build a gear shape and model a gear-to-gear contact
- Gear tooth profile is automatically created based on parametric inputs
- Toolkit automatically creates contacts
- Gear can be a rigid body or flexible body

Disadvantages:

- Results must be visualized at calculated times, and not interpolated between two steps

2.1.6 Signal processing and time frequency analysis

Time-domain data consists of one or more input variables and one or more output variables, sampled as a function of time. Frequency-domain data consists of either transformed input and output time-domain signals or system frequency response sampled as a function of the independent variable frequency. Fourier transformation approximates every periodic signal using harmonic functions with discrete frequencies. This helps to analyse the frequency content of any signal. In other words, Fourier transformation converts a time-domain data into a frequency-domain data. Fast Fourier Transform (FFT) is one of the algorithm that is used for computing discrete Fourier transformations(or its inverse) of a sequence of data. Any signal that converted for Fourier analysis may be represented or approximated by sums of simpler trigonometric functions. Machine vibration is typically analysed with measurements of the displacement, velocity, and acceleration. These measurements are, however, time domain measurements, meaning their amplitudes are plotted versus time. But these signals contain useful information, such as noise and harmonic content, that are difficult or impossible to detect when their amplitudes are plotted in the time domain. FFT helps in understanding these vibrational signals by identifying variations in amplitude at certain frequencies.

Short-time Fourier transform (STFT) for discrete data is Fourier transform of data broken up into chunks or frames. These chunks . It is used to analyse the variation of the sinusoidal and phase contents of a signal over time.

2.2 State of the art

Topics to be discussed:

- Examples from the literature
- Actual tests and results
- Order tracking as a method to detect gear faults
- Further tooth crack detection techniques

3 Objectives

The main aim of this work is to properly simulate the dynamic response of a three-spur-gear transmission system under different constant angular acceleration conditions within specified time frames by making use of the Ansys Motion drive train Toolkit.

In order to verify that the simulation was set up and performed correctly, different data will be collected on specific locations of the system and then analysed according to the theoretical knowledge of chapter 2. In the same manner, self-calculations will allow a mathematical comparison with the theory and the validation of the simulation.

4 Hypothesis

Since no external disturbances are planned to be applied to the system, the simulation results are not expected to deviate considerably from the calculated values. All kinematic data (position, velocity and acceleration, both translational and angular) on the specified markers should behave either in a constant, linear or sinusoidal manner depending on the acceleration input on the pinion and this should comply with the behaviour of a harmonic motion, as seen in subchapter 2.1.1.

Only during the sudden change of acceleration conditions a deviation from a predictable state (i.e. steady, at rest) is to be expected. Any other kind of variation of the periodic or constant signal content can only be justified by the dynamic phenomena produced by the gear meshing. These perturbations should be explained through the existence of a possible realistic fault in the transmission system within the simulation time frame. Nonetheless, based on the load conditions of chapter 5.3, the only effects that could play a role here are the transmission error and the imperfect impact from the tooth contact. The overall behaviour of the system should also be clearly noticeable in the frequency domain, where the shaft and gear mesh frequencies play a major role.

5 Method

In order to have a complete picture on how the simulation was carried out, the methodology is divided and clarified in different sections.

5.1 Set up

The gear transmission system to be studied consists of a single set of three coupled spur gears. Essentially, this system is a simplified representation of the actual testing bench that has the purpose of performing meaningful tests on planetary gears in an individual basis. According to the actual planetary gear train for which the testing bench is planned, the input, idler and output gears can also be labeled as drive sun, planetary and driven sun gear, respectively. The full assembly done in Ansys Motion is shown in Figure 4.

The geometric dimensions and characteristics of the proposed drive train are based on the actual testing components, although with some simplifications. The main set of features of the system is to be found in Table 1 (for other parameters not mentioned here, default software values were used). Figure 5 depicts most of these key variables and parameters too.

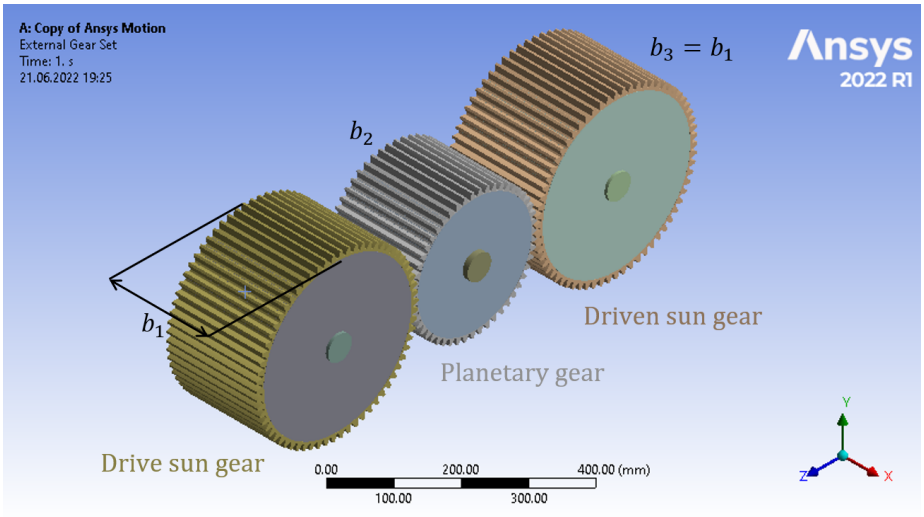

Figure 4: Gear set up, isometric view. Definition of the labels and widths of the gear set model in the Ansys Motion Workbench environment.

Table 1: Gear set parameters.

Parameter	**Symbol**	**Gears 1/3**	**Gear 2**	**Unit**
Module	m	5		-
Pressure angle	α	20		°
Centers distance	a	292.5		mm
Material	-	Steel C45E (1.1191)		-
Number of teeth	z	66	51	-
Gear width	b	190	180	mm
Angular velocity	n	2781.82	3600	rpm
Torque	T	6470.59	5000	Nm

With the drive train Toolkit it is possible to create the gear geometries by defining the key parameters as an input within the different software functionalities. Even though the program is capable to perform MBD simulations by also considering the assembly of bearings and a gearbox housing, these components were neglected to keep the model as simple as possible, thus making an analytical approach more feasible. In order to constrain the movement of the gear set, the toolkit creates the necessary joints between components; in this case gear and shaft, and the gear meshing (tooth contact). The only remaining task is to manually create a revolute joint between the shafts and the ground. Because the role of the shafts beyond defining the movement type is of no relevance, their dimensions are trivial for this simulation (as long as they allow a proper visualization of the model).

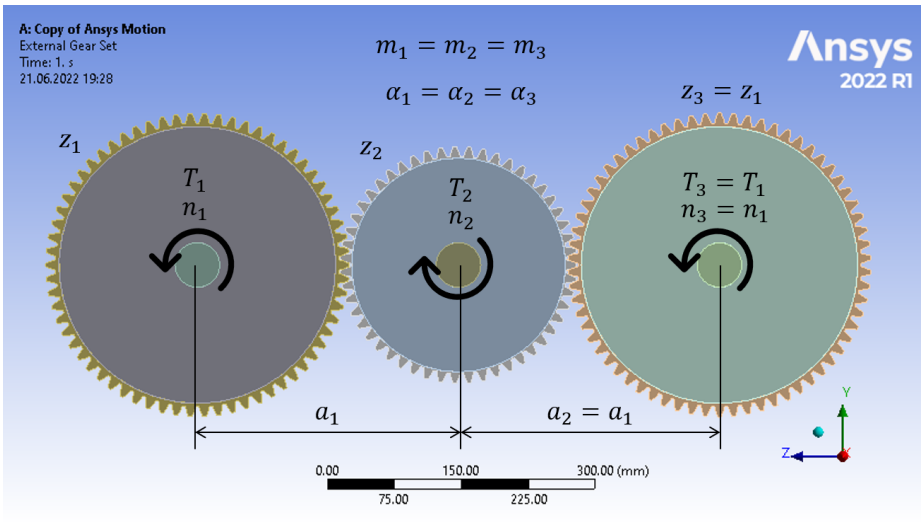

Figure 5: Gear set up, front view. Definition of the key measures and parameters of the gear set model in the Ansys Motion Workbench environment.

Details of "External Gear Set"

Definition	
Type	ExternalGearSet
Gear Profile Generation	Program Controlled
Suppressed	No
Type of Gear	Spur
Module	5 mm
Pressure Angle	20 °
Idler Gear	Use
Reference Point	Program Controlled
Use Advanced Option	Use
Advanced Option	Gear Advanced Option
Initial Angle	0 °
Center Distance	
Driving to Idler (Ideal)	292.5 mm
Idler to Driven (Ideal)	292.5 mm
Driving	
Name	Gear1
Quality	6
Number of Teeth	66
Face Width	190 mm
Addendum Coefficient	1
Dedendum Coefficient	1.25
Profile Shift Coefficient	0
Tool Tip Radius	0.2 mm
Use Modification	None
A Point	173.832128966049 mm
B Point	82.0286340926787 mm
Z Point	105.014639503486 mm
Web	Program Controlled
Tooth Stiffness	FE Method
Tooth Stiffness Result	Tabular Data
Idler	
Name	Idler
Quality	6

Tooth Stiffness Result	Tabular Data
Idler	
Name	Idler
Quality	6
Number of Teeth	51
Face Width	180 mm
Addendum Coefficient	1
Dedendum Coefficient	1.25
Profile Shift Coefficient	0
Tool Tip Radius	0.2 mm
Use Modification	None
A Point	121.316799254185 mm
B Point	82.0286340926787 mm
Z Point	105.014639503486 mm
Web	Program Controlled
Tooth Stiffness	FE Method
Tooth Stiffness Result	Tabular Data
Driven	
Name	Gear2
Quality	6
Number of Teeth	66
Face Width	190 mm
Addendum Coefficient	1
Dedendum Coefficient	1.25
Profile Shift Coefficient	0
Tool Tip Radius	0.2 mm
Use Modification	None
A Point	173.832128966049 mm
B Point	82.0286340926787 mm
Z Point	105.014639503486 mm
Web	Program Controlled
Tooth Stiffness	FE Method
Tooth Stiffness Result	Tabular Data
Material	
Assignment	C45E (1.1191)

Details of "Gear Advanced Option"

Definition	
Suppressed	No
Thin Slice	User Defined
Number of Thin Slices	90
Force for Tooth Stiffness	10 N/mm
Number of Involute Points	30
Number of Trochoid Points	6
Friction Coefficient	0
Static Friction Coefficient	0
Dynamics Threshold	150 mm/s
Stiction Velocity	150 mm/s
Contact Damping Ratio	0.001

Figure 6: Options used in ANSYS Motion

5.2 Assumptions

Once the gear set up is properly defined and constrained, it is important to also establish the appropriate physical boundaries within the context of the simulation scope. To achieve this, the following assumptions and simplifications are taken into consideration:

- The gear set consists only of spur gears (no helix angle).
- The gears present no geometrical corrections (micro-geometry).
- The gear material is isotropic and does not have a hardening surface.
- The shafts and gear webs are modeled as rigid bodies.
- The gear teeth are modeled neither as rigid nor flexible bodies, they follow the slice calculation method incorporated in the Ansys Motion software.
- The input power is always constant and directly provided to the shaft of the drive sun gear.
- Energy is completely conserved along the whole transmission (no losses of any kind).
- None of the components are defective.
- The shafts are always in a fixed position with respect to the ground.
- The global coordinate system is the one provided by the Ansys Workbench environment (see Figure 4).
- The geometrical centers of the gears are aligned in the planes ZY and XZ.

5.3 Load conditions

The definition of the loading conditions is set up with aid of a drive train feature known as Driving Scenario. As already mentioned, two angular acceleration conditions are to be investigated, nevertheless both will be simulated within the same sample. By setting the initial conditions of constant torque on the driving shaft, the system starts from rest with a zero angular velocity that will linearly increase for two seconds (at a constant angular acceleration) until attaining the final maximum value of Table 1. After the transient response, the angular velocity will remain constant in a steady state condition (no angular acceleration) for three seconds, giving a total simulation time of five seconds.

Details of "Drivetrain Driving Scenario"

Definition	
Suppressed	No
Input	
Input Shaft	Shaft
Input Speed Type	Acceleration
Rotating Direction	Counterclockwise
Input Power Type	Constant
Input Power	1884995.59215 W
Max Moment	6470590 N·mm
Duration	2 s
Start Speed	0 rpm
End Speed	2781.82 rpm
Interpolation Type	Specify Number of Interpolation Data
Number of Interpolation Data	100

Figure 7

5.4 Simulation settings

Important fact: The output step (sample rate) was of 3000 samples per second. The GMF is of 3060 Hz, so it could never be detected in the simulation results, see Ansys presentation

Details of "Analysis Settings"

Simulation Controls	
Simulation Type	Dynamic analysis
Include Static Analysis	No
Include Modal Analysis	No
Number Of Threads	1
Step Control	
End Time	5 s
Output Step	3000
Synchronize Maximum Step Size To Output Step	Yes
Solver Controls	
Solver Type	Program Controlled
Treat of Non-Contact Entity	Ignore in Chained System
Skip Initial Analysis	Pos. Vel. Acc
Use The Number Of Steps In Initial Position Analysis	No
Relative Error	0.0005
Output Control	
Create Graphics Files	No
Create Plot Result File	No
Record Stress/Strain	Yes
Record Constraints	Yes
Record Forces	Yes
Record Contacts	Yes
Record Sub-Entities	Yes
Record Frequency Response	No
Dynamic	
Error Tolerance For NR Convergence	0.001
Numerical Damping	1
Initial Step Size	0.0001 s
Maximum Step Size	0.01 s
Minimum Step Size	1E-08 s
Step Size factor	2
Maximum iteration For Step Size Control	10
Use Stabilization Time	None
Units	
Postprocessor Units	Convert to Motion-specific (mm kg N s rad)
Analysis Data Management	

Figure 8

5.5 Measurement technique

In ansys motion, the inspection of the gears is carried out only in defined marker locations. Usually, these marker locations are automatically defined by the software. In our case, one of the markers used was set up automatically by Ansys (Marker B) and the other marker was manually added (Marker A). Locations of both the markers is shown in the figure 9. Dimensions of the markers are specified in the figure. Measurements of kinematic and dynamic parameters at these points is used for analysis of the motion and vibration of the gear train.

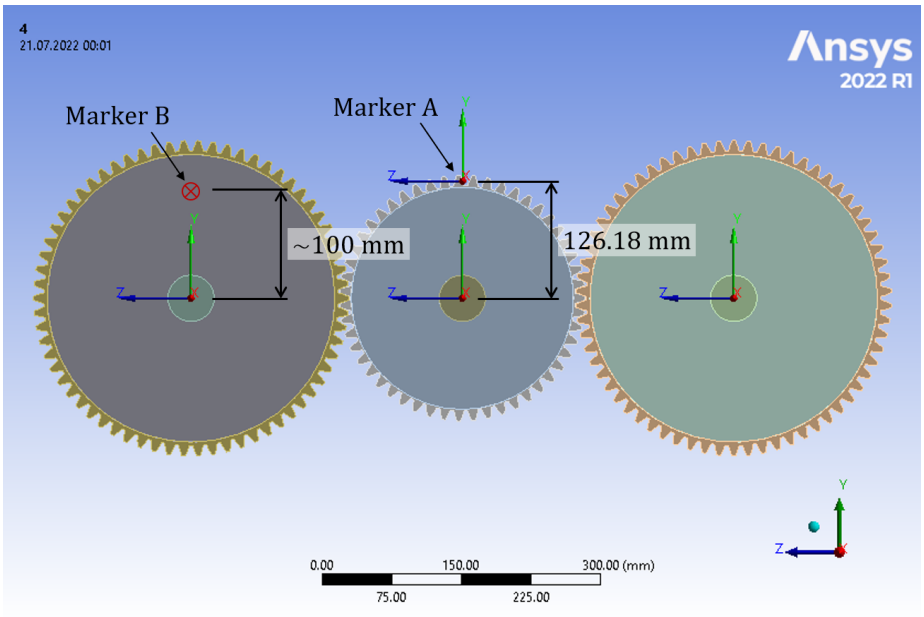

Figure 9: Gear set up, front view. Definition of the measurement markers located on A, a tooth at the planetary gear, and B, a default position at a distance from the center of rotation of the drive sun gear.

5.6 Procedure

- Load conditions applied, simulation performed.
- Time domain analysis, comparison between gears and gear pairs
- Frequency domain analysis, always at periodic signals FFT, STFT. Comparison between components, markers
- Hints for the frequency domain signal processing:
  - FFT - Type: Magnitude, Scale: Original when peaks are easy to notice, dB when low amplitudes matter (i.e. at really high freq.),

Window: Hanning, number of points determines up to which frequency we want to see the spectrum (many points, more freq.), start: 3s, end: 5s because here the behaviour is stable

- STFT - Sampling frequency: Maximum frequency we want to see (recommended to try at low and high frequencies to see different effects), time slice: around 0.5s (bigger slice = better vertical resolution, lower slice: better horizontal resolution), overlap: 99 (better resolution but more uncertainties as results of different time slices are merged with each other), nFFT: as high as possible for better resolution, start: 0, end: 5 so whole run time is visualized, scale: dB to detect noise

*Before showing the results it was pretended to make the relevant calculations (for example kinematic data, gear forces) using the information and formulas provided in the theory, so a comparison with the simulation is plausible for those values. So far the results can be found in Excel.

6 Results and discussion

This chapter presents some of the most relevant data that can be extracted from the Ansys Motion Post-processor. It makes use of different signal processing tools for the time and frequency domain analysis in the form of FFTs and STFTs, that will allow the postulation of different hypothesis and conclusions that could provide a better idea of what happens to a certain component (i.e. planetary gear, input power shaft) or the system as a whole under a certain load condition at a specific point in time or during a meaningful time span. The discussion made on each element is based on the observed results of the graphs and plots and the theoretical background provided in chapter (2).

Before starting with the analysis, it must be clarified that some of the measured signals are of very low value in comparison to the magnitude of the main parameters of the system (for example, small deviations of the angular acceleration with respect to the actual angular acceleration vector). When that is the case, the frequency amplitudes of the curves in the FFT charts or the intensity in a Campbell plot could actually be neglected, as it is difficult that they could truly interfere with the optimal performance of the machine with such barely detectable effect. In spite of that, the behaviour and evolution of these results can provide an insight of what could happen to the system on a greater scale with bigger excitations or faults. Taking this into consideration, it can come to the case that the actual numerical values of some figures are not analysed and just a qualitative assessment is sufficient to suggest or propose a statement regarding the simulation.

A last remark is that all FFTs performed are performed beginning on the third second of the simulation, since this corresponds to a period of time where the frequency of the signals is stable and therefore allows a better frequency domain analysis of the steady state dynamics. For the STFTs it is important

to view the whole transient behaviour and at least have a glimpse when the angular frequency turns constant.

6.1 Kinematics

In this section the simulation results of the kinematic data are shown and discussed. For all relevant variables, the main focus is first set on the planetary gear, due to the fact that the most important measures belong to it in a testing bench application context. When it is relevant for the analysis, the results of the drive sun are also highlighted and compared. However, because of the idealized conditions of the system (see chapter 5.2), the results obtained for the second sun gear (driven) are practically the same as for the driver and therefore are neither shown nor discussed any more.

6.1.1 Linear

Displacement In the gear set up proposed in this report two different scenarios were simulated: first a linear increase of the angular frequency over time and, immediately after, a constant value of it maintained for a second time frame. Based on the scope established in chapter 3, it is important to define that only the constant angular velocity condition is meaningful for the linear kinematic analysis whereas the transient state has more importance for the vibrational (subchapters 6.1.1 and 6.1.2) and dynamic (chapter 6.2) response of the system.

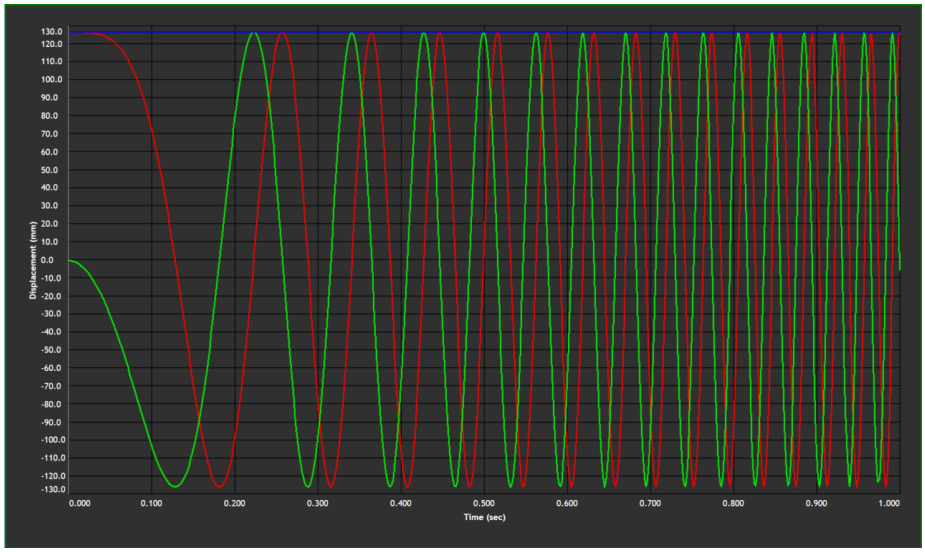

Figure 10: Variation of the linear displacement of the planetary gear over time (0 to 1 seconds). Red: y-component, green: z-component, blue: magnitude.

As described in chapter 2.1.1, the linear displacement of a point fixed in the circumference of a rotating circular body behaves in a periodic way and can be

fully depicted by two of its three axis components and the resultant magnitude of them. For this set up (Figure 5) the radial displacement in the x direction has a negligible value for all gears (consequently also for the velocity and acceleration), which is acceptable as it is something that could be expected. Nevertheless, it is interesting that it is not completely zero (but that will be discussed later).

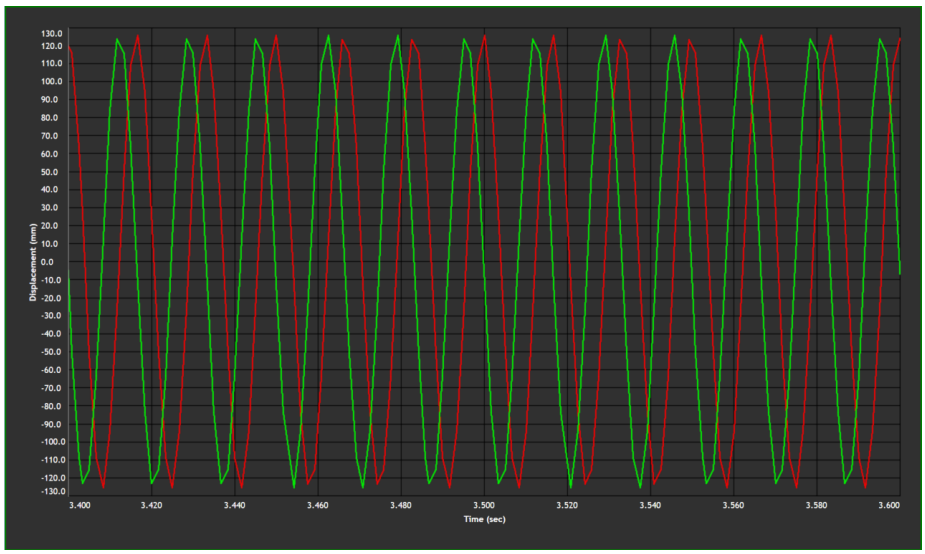

Figure 11: Variation of the linear displacement of the planetary gear over time (3.4 to 3.6 seconds). Red: y-component, green: z-component.

The first results obtained correspond to the y and z displacements of the idler gear's tooth (Figures 10 and 11). By checking the sinusoidal characteristics of the functions, particularly during constant angular velocity (Figure 11), it is clear that the maximum amplitude corresponds to the point where the marker was initially set and the frequency is held constant over time, so a mathematical representation would be accurate if equations 13 and 16 were employed to model this behaviour. Unfortunately, the angular velocity of the gear is so high that, with the applied sample rate, some accuracy is lost. This can be noticed in the low quality of the curves near the upper and lower peaks. By comparing this level of detail with the one observed during the period of linear increasing of the angular velocity as in Figure 10, it can be concluded that the problem is caused mainly by the sample rate, because within the simulation first instants (lower angular frequencies), the peaks are reproduced with better resolution until they cannot be properly sampled anymore.

Additional to this, if a closer look is taken at the magnitude value (Figure 12), it can be seen that in reality it is not constant over time but oscillates in a periodic manner as well. Although this behaviour is only shown for a couple of milliseconds, it is true for all the simulation time. Within the first two seconds (from zero to constant angular frequency) it even has the sample resolution

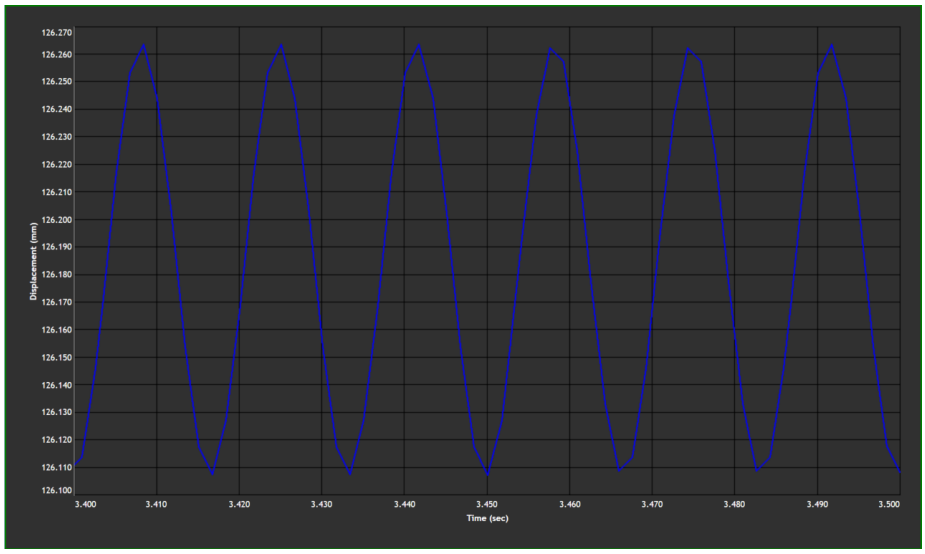

Figure 12: Variation of the linear displacement magnitude of the planetary gear over time (3.4 to 3.5 seconds).

improvement that was previously commented. This fact may mean that the origin of this effect is not caused by an improper sampling. Different sample frequencies should be implemented to clarify this, though.

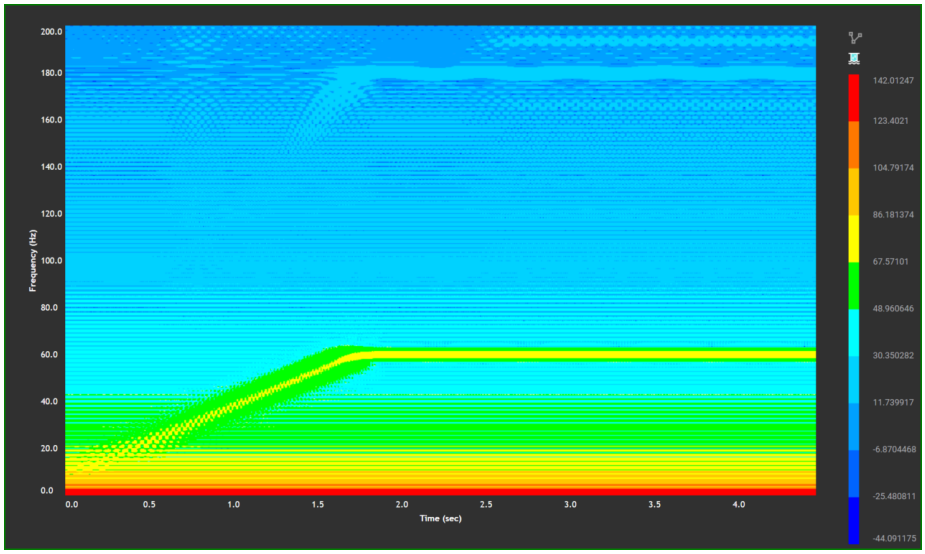

Figure 13: Colormap (STFT) plot of the linear displacement magnitude of the planetary gear. Amplitude values shown in decibel scale.

Another possible explanation to the varying magnitude could be a perturbance in the system in the form of a vibration. To have a better inspection at it, a STFT is performed for this curve. In the resulting colormap of Figure 13 we can see a linear increase in frequency over time until the constant shaft angular speed at 60 Hz is reached. If such frequency were not visible, the magnitude of the displacement should always remain constant, thus describing the rotation of a motion that is perfectly circular. But because this is not the case, it can be interpreted that the trajectory described by the motion is slightly different from a circle. This could either mean that a small deformation of the tooth takes place each time the gear rotates or that the marker is not fully fixed in its position at the tooth location.

Velocity The linear velocity curve (Figure 14) can serve as a method to verify that the kinematic simulation was performed correctly. For a constant magnitude, the behaviour of the functions in the y and z directions is similar to the displacement as equations 14 and 17 suggest, being the amplitude value, one of the main differences to be encountered. Because the frequency is the same as in the displacement (but just out of phase with each other), the sample resolution inconveniences are present again. Furthermore, the magnitude value is now a periodic signal conformed by several harmonics, but this is something that will be treated in the following section.

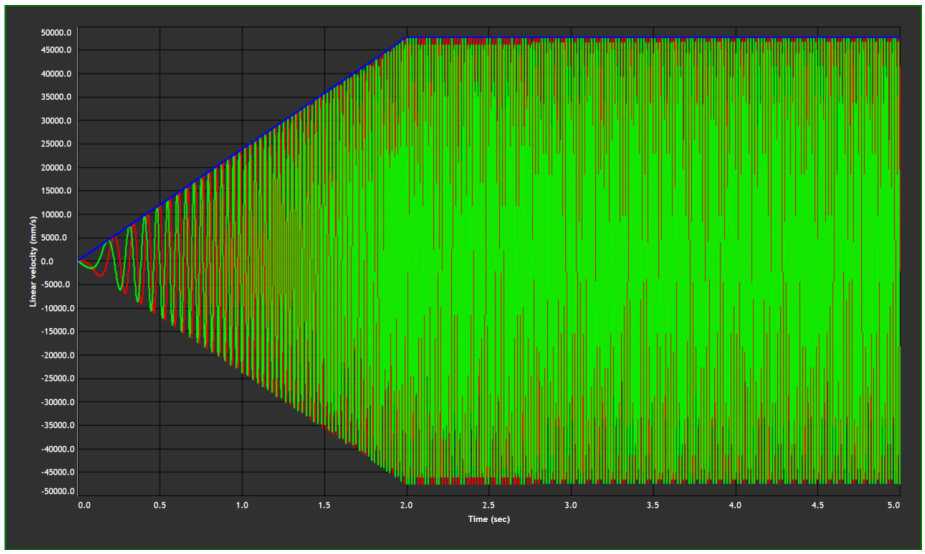

Figure 14: Variation of the linear velocity of the planetary gear over time. Red: y-component, green: z-component, blue: magnitude.

Acceleration Even though displacements and velocities can be measured to study the vibrational effects of a system, another approach consists on analysing

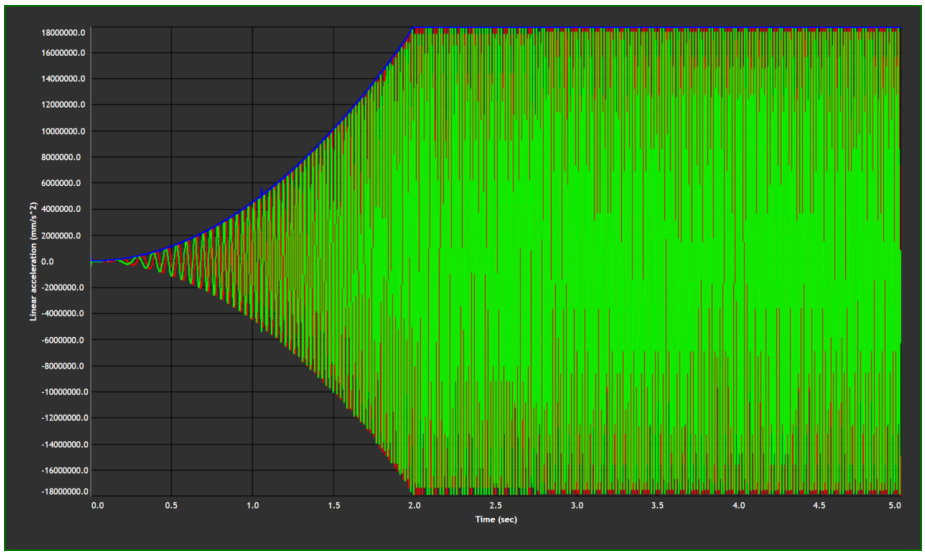

Figure 15: Variation of the linear acceleration of the planetary gear over time. Red: y-component, green: z-component, blue: magnitude.

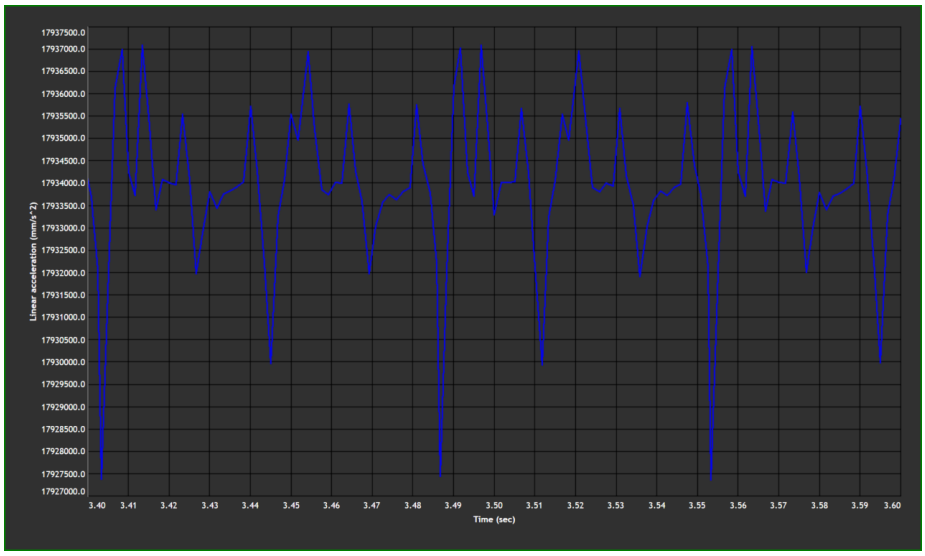

Figure 16: Variation of the linear acceleration magnitude of the planetary gear over time (3.4 to 3.6 seconds).

the accelerations, as they offer a more sensitive insight on this phenomenon. On the one hand, considering that vibrations appear as periodic functions with certain frequencies, the amplitude acceleration values are the ones with

higher order of magnitude and could therefore allow a better understanding on the possible problems that cause undesired performance, particularly at higher frequencies. On the other hand, as also seen in chapter 2.1.3, the selection of the parameter of study in vibration analysis strongly depends on the frequency of the signal, so reading this data could limit the findings on the shaft frequencies (46.364 Hz and 60 Hz) and just give a clear picture about the gear mesh frequency (3060 Hz). For our simulation results, acceleration will be the variable of special interest because it is the most common measured variable for this kind of systems according to several examples from the literature. [27] [28] [29]

In Figure 15, the linear acceleration of the planetary gear is shown in its y and z components. The behaviour again is the one expected from the theory, so the curves are just multiples of the displacement functions (but only during the steady state phase). For the first two seconds, the quadratic increase of the magnitude is clearly visible and then stabilizes. As it reaches a final maximum constant value, we can take a deeper look and observe a periodic signal with specific harmonic content in Figure 16.

Before proceeding with the analysis of the previous signal, it is also interesting to check out the results of the marker placed in the drive sun gear (Figures 17 to 19). The acceleration curves of this pinion should evolve in an equal manner as with the planetary gear with the difference of having another angular frequency and maximum amplitude, following the proper transformations from the theory seen in chapter 2.1.1. This is also valid for the displacement and velocity graphs. Surprisingly this does not occur exactly like that as we observe in Figure 17, which shows curves that have a lot of unexpected peaks and noise along the signal.

During the acceleration increase phase (Figure 18), the disturbances are predominant in specific time frames (i.e. between 0.1 and 0.3 seconds) and barely seen at other moments (from around 0.32 to 0.5 seconds). From a very first impression, it can be said that the noise detected within this period corresponds to a rattle noise. According to the theory revised in chapter 2.1.3, this is a low frequency impulsive noise product of gear contact backlash and load fluctuation or varying driving torque. While the first point is possibly true and causes an impulsive mesh force due to an unstable one-sided contact, the second one should be better revised in the torque graphs from subchapter 6.2.2. Another aspect to highlight is the appearance of extremely high peaks of very short duration. These could announce the presence of stronger rattle effects during the RPM linear increase but this should not yet be declared as such until further results are discussed.

Looking at the constant angular velocity phase, the acceleration curves of Figure 19 show again that the sample rate is not adequate for this shaft frequency, even if it is lower than in the planetary gear. Because the amplitude order of the acceleration is significantly higher than the one of displacement or velocity, there is also a clear degradation of the resolution, specially near the peak values. As a result, a non-constant acceleration magnitude produced (Figure 20).

The acceleration magnitudes of the driving (Figure 20) and idler (Figure

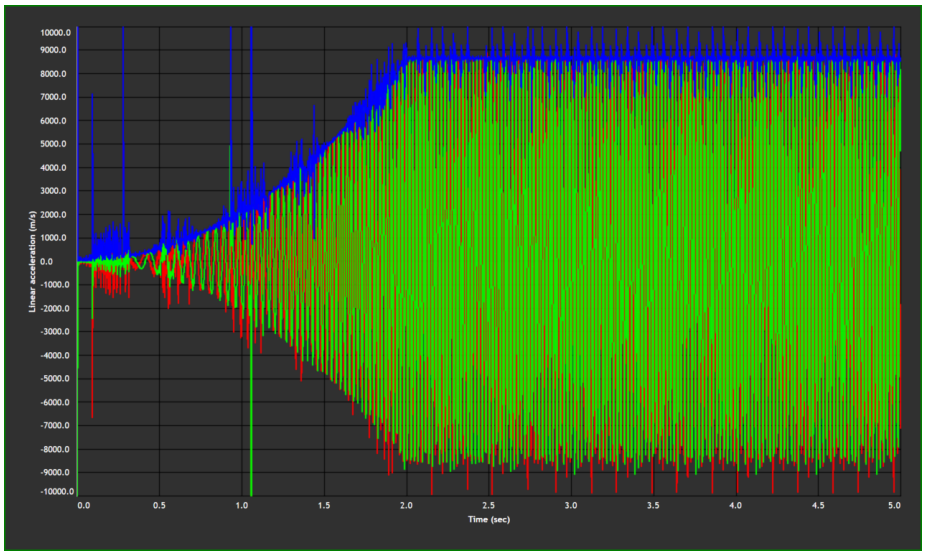

Figure 17: Variation of the linear acceleration of the drive sun gear over time. Red: y-component, green: z-component, blue: magnitude.

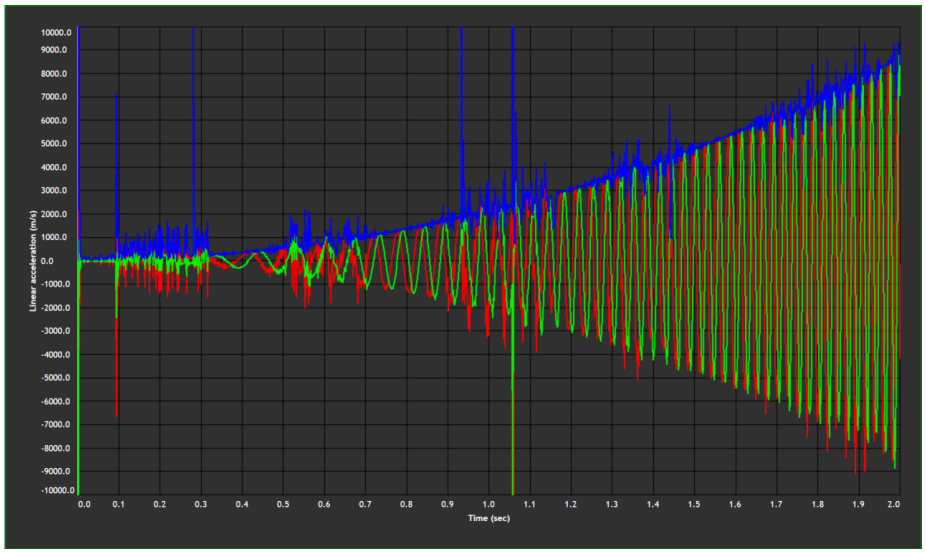

Figure 18: Variation of the linear acceleration of the drive sun gear over time (0 to 2 seconds). Red: y-component, green: z-component, blue: magnitude.

16) gears can be parallel discussed. From both graphs it is clear that there are harmonic components, but whether they are a result of whine noise or improper sampling is still a question to be answered. By performing a FFT of

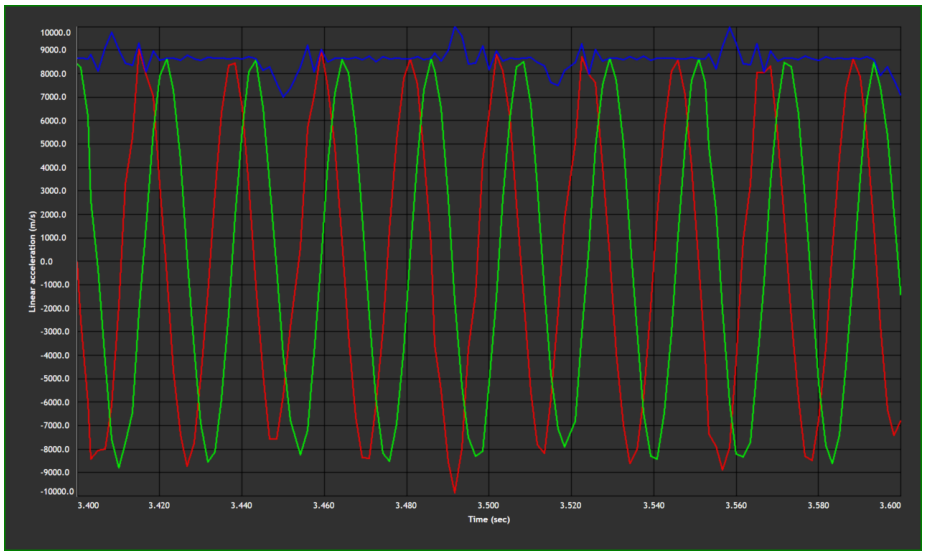

Figure 19: Variation of the linear acceleration of the drive sun gear over time (3.4 to 3.8 seconds). Red: y-component, green: z-component, blue: magnitude.

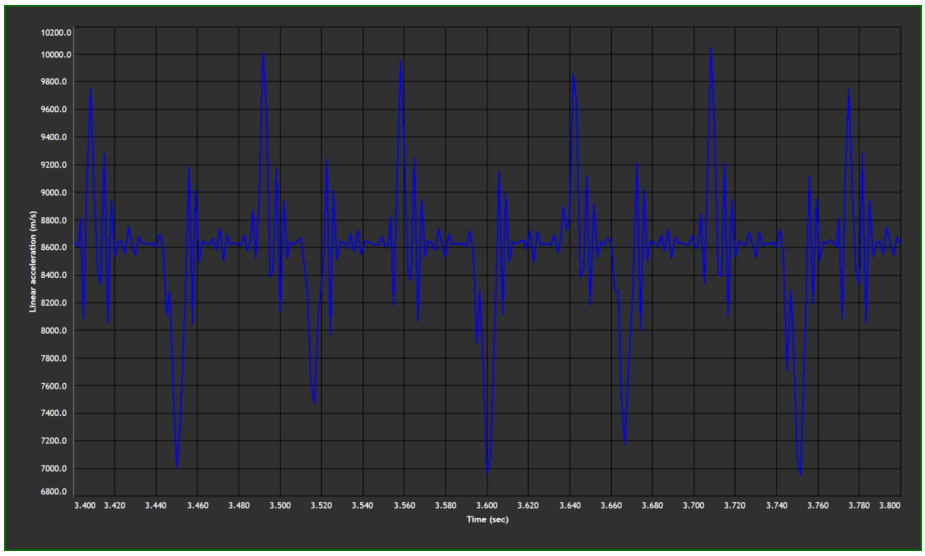

Figure 20: Variation of the linear acceleration magnitude of the drive sun gear over time (3.4 to 3.6 seconds).

both curves, the harmonic content can be now clearly distinguished as seen in Figures 21 and 22. For the planetary as well as for the sun gear we see the expected shaft frequencies with a high amplitude value. However, in none of

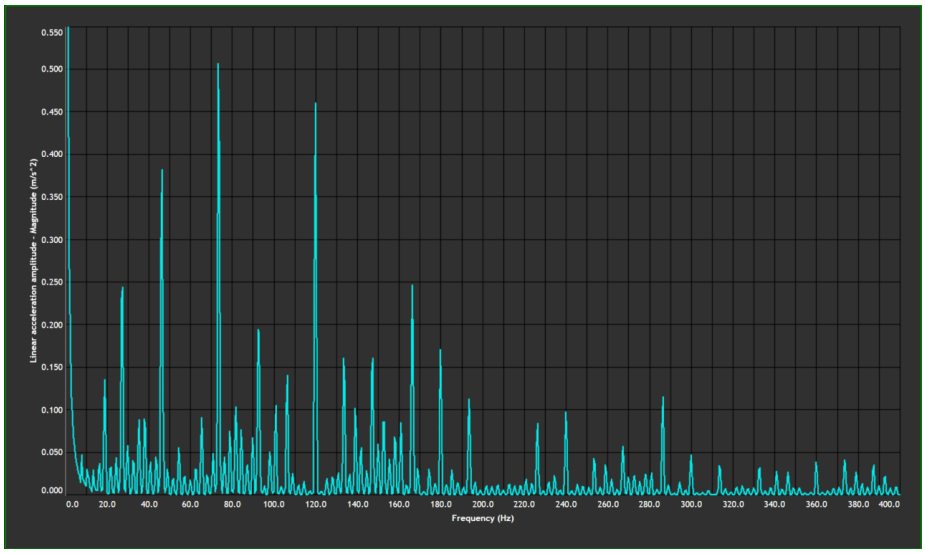

Figure 21: Frequency spectrum (FFT) of the planet's linear acceleration magnitude (up to 400 Hz).

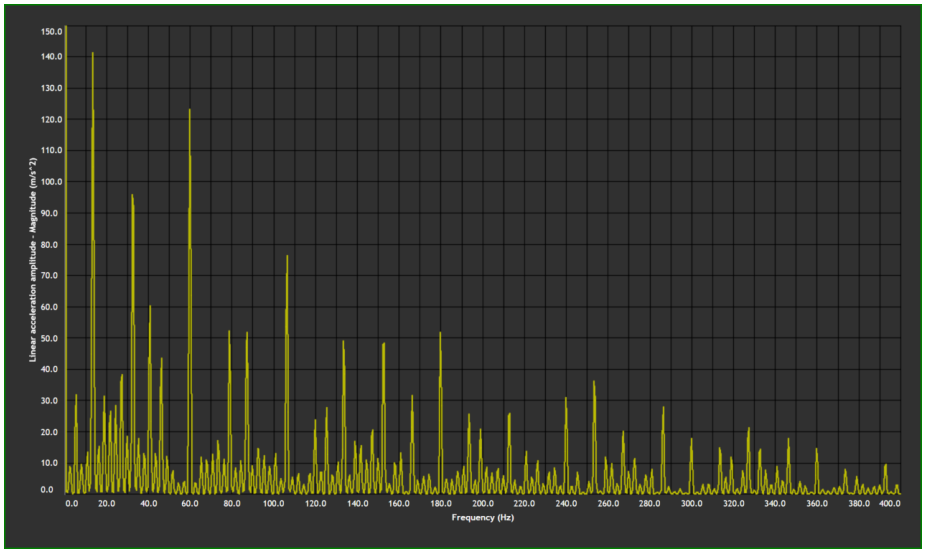

Figure 22: Frequency spectrum (FFT) of the sun's linear acceleration magnitude (up to 400 Hz).

the bodies, are these frequencies the most predominant of the spectrum. In the planetary gear, a gradual decrease of the intensity of the frequency content can be perceived, here the most relevant frequency is around 13 Hz. At the drive

sun marker, frequencies of 73 Hz and 120 Hz (two times the idler´s angular frequency) are shown as more prevalent in the signal than the one of the ones of the actual rotating body. In a classical MBD analysis, each frequency should correspond to the vibration of specific components (i.e. bearings, housing) and a high amplitude of a specific frequency in the FFT curves suggests a possible fault of the body that is associated with that frequency. But because our system is only composed of 6 bodies and a total of two different angular frequencies among them, there is no clear clue about what could generate such a diverse FFT spectra.

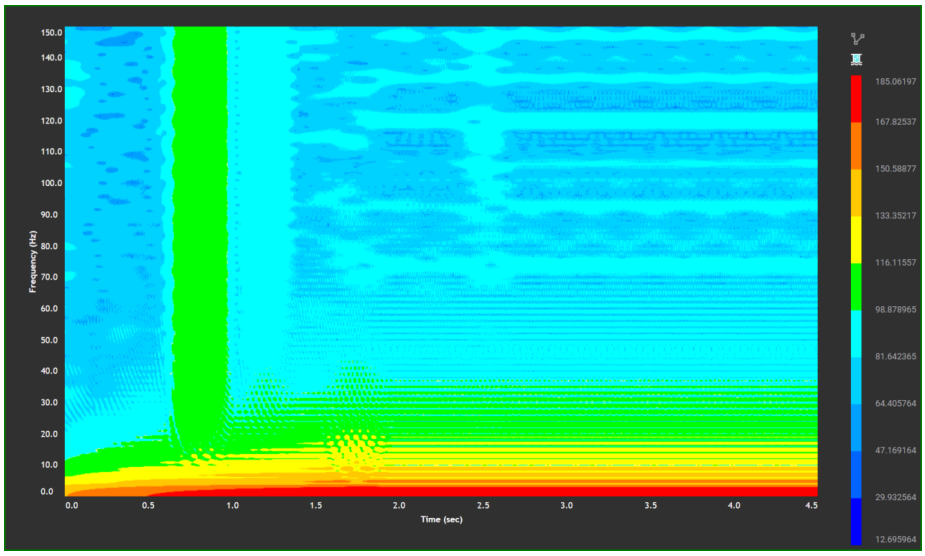

Figure 23: Colormap (STFT) plot of the linear acceleration magnitude of the planetary gear. Amplitude values shown in decibel scale.

If we observe the evolution of the frequency composition over time in the STFTs of Figures 23 and 24, the main frequencies remain practically constant for the steady state condition and they agree with the results of the FFT graphs. In both diagrams, it is important to notice a vertical line with a particular elevated amplitude value at around 0.8 seconds. In a colormap this effect means that at a certain point in time, the gear has reached an angular velocity such that an uncommon acceleration peak occurs for any frequency. Because this happens for both gears at the same time, it is highly possible that it is related to unnatural strong impacts along the transmission.

To conclude with the linear acceleration analysis it is valuable to have in mind that the x-component of this variable is not completely zero for any of the gears, as seen in Figure 25. But since these curves do not describe any sort of periodicity, they can be neglected for this time as they might just be irregular noise (maybe product of some simulation residual error).

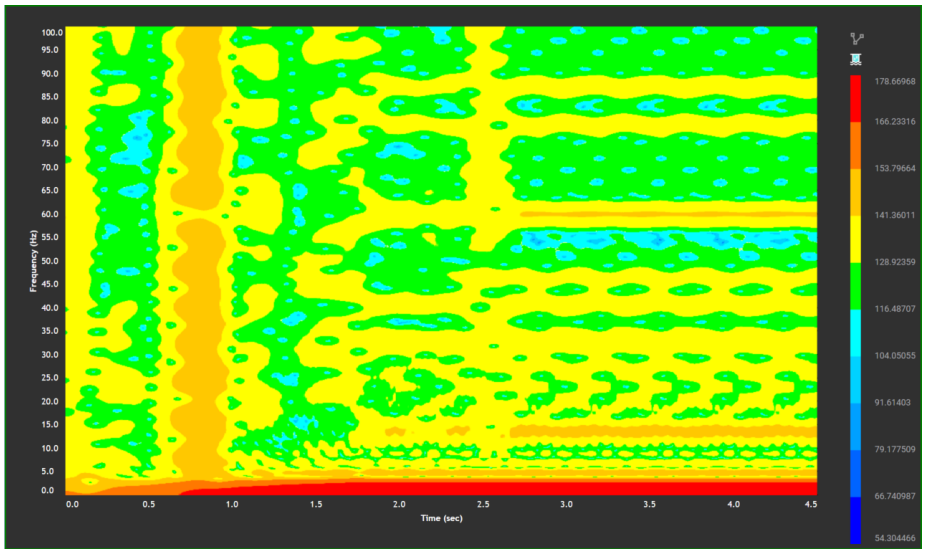

Figure 24: Colormap (STFT) plot of the linear acceleration magnitude of the drive sun gear. Amplitude values shown in decibel scale.

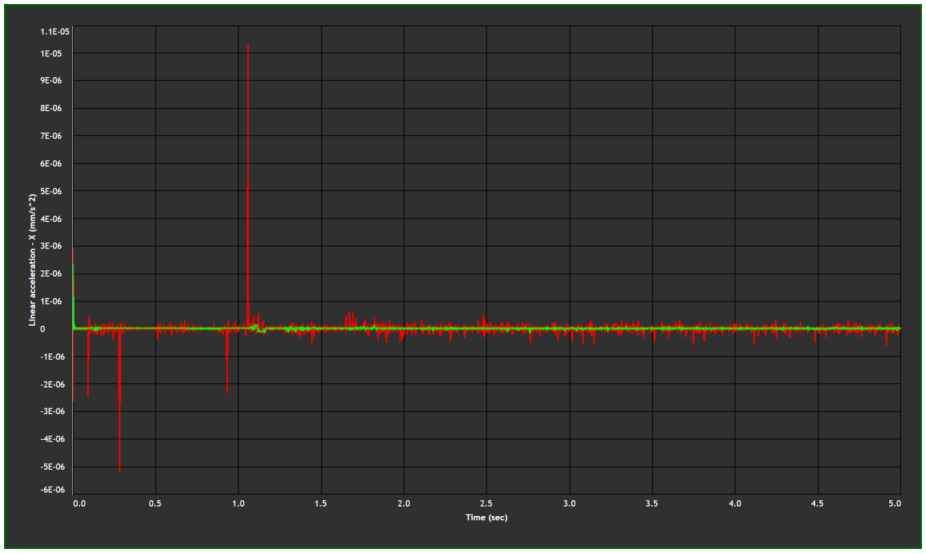

Figure 25: Variation of the linear acceleration x-component over time. Red: planetary gear, green: drive sun gear.

6.1.2 Angular

Displacement More in an informative sense, the angular displacement function of the planetary gear helps to verify that the set up was made correctly by

comparing this result with the analytical solution. Figure 26 is congruent to the result that can be obtained using equation 12 when the angular velocity input of the system is known. Here a quadratic increase of the total angle takes place the first two seconds and then becomes a linear function once ω is constant. From this chart it is known that during the simulation runtime the planetary gear completes 240 full revolutions.

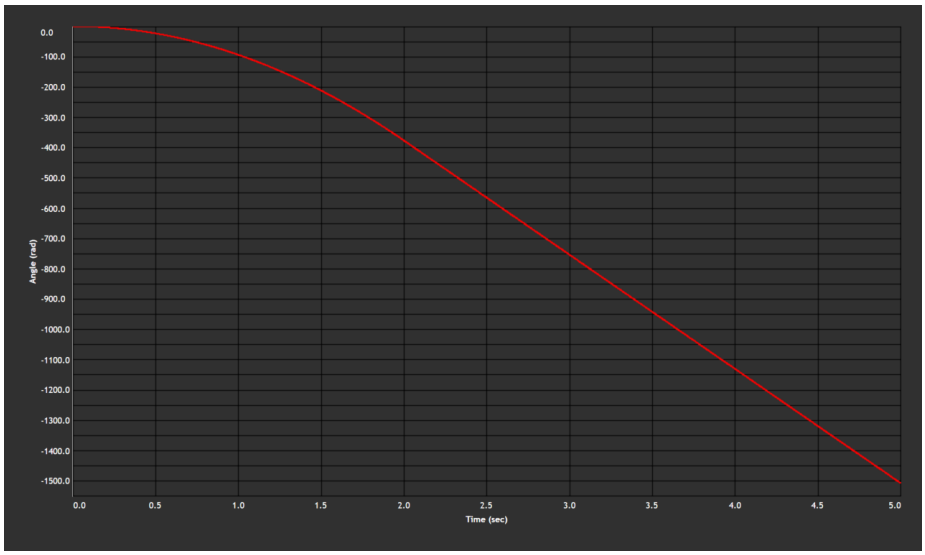

Figure 26: Variation of the total angular displacement of the planetary gear over time.

Velocity Although the angular velocity of both gears was given as an input to the problem formulation and its behaviour was constrained according to chapter 5.3, the right set up of this load scenario can be verified from the post-processor environment and at the same time certify the validity of equation 10. In this sense, Figures 27 and 28 serve as an illustration of the initial conditions of the system and show the correct gear mesh coupling of the pair created within the drive train Toolbox, because the angular velocity of the planetary gear is, in fact, a multiple of the gear transmission ratio, just as the theory suggests.

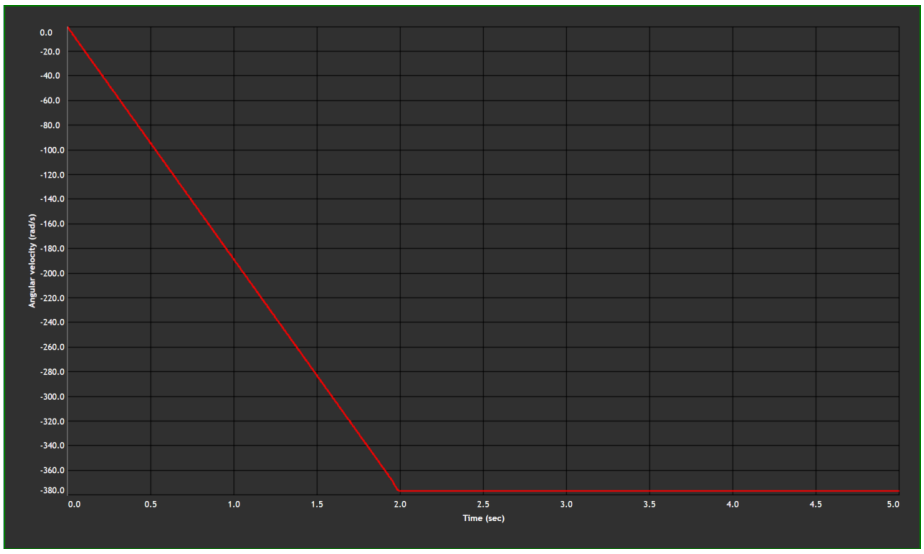

Figure 27: Variation of the angular velocity of the planetary gear over time.

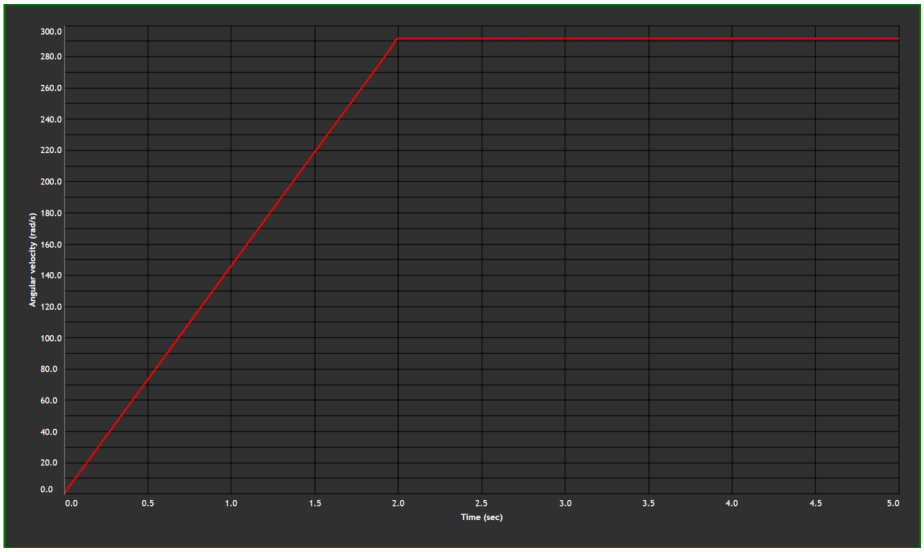

Figure 28: Variation of the angular velocity of the drive sun gear over time.

Acceleration For the previous two angular variables it was seen that the simulation results are well-defined smooth curves that accurately describe the kinematic behaviour of the gears. Following the same logic, the acceleration graphs should show functions of constant value and a step change after two seconds (once the conditions are changed), but that is not entirely the case.

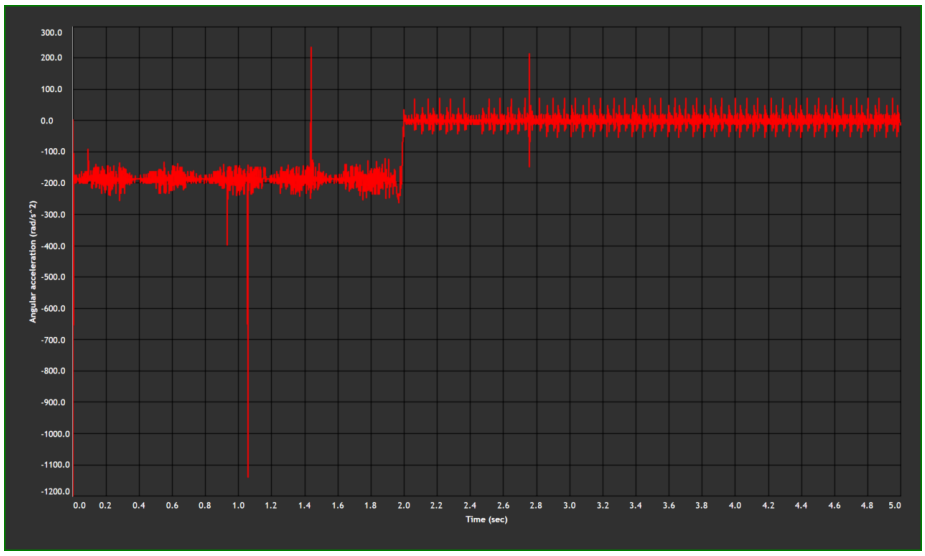

Figure 29: Variation of the angular acceleration of the planetary gear over time.

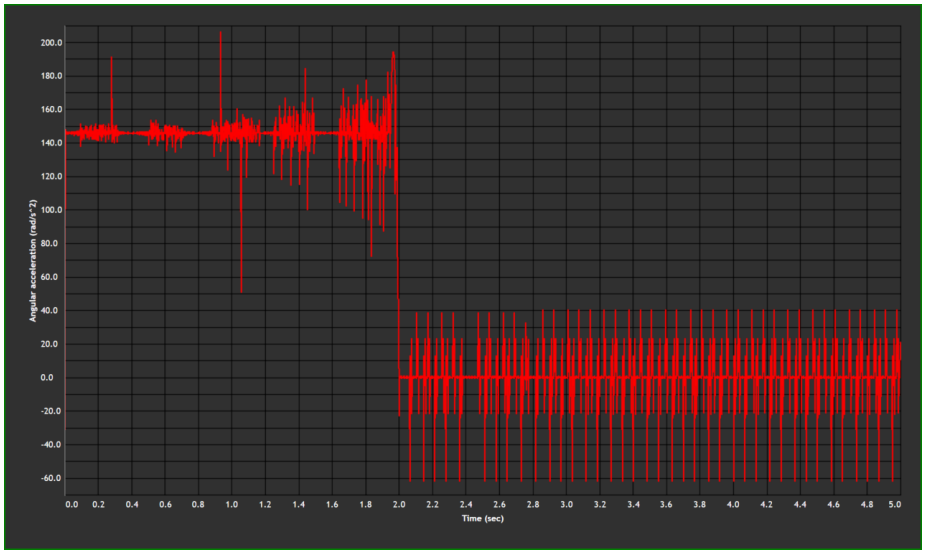

Figure 30: Variation of the angular acceleration of the drive sun gear over time.

Though it is not common to interpret signals from the angular kinematics as part of a vibration analysis, figures 29 and 30 are worth of discussion. When setting up a drive train model in Ansys Motion it is not possible to enter directly an angular acceleration in the loading conditions; instead of it, a function of the velocity is the one given. It is inferred that a value of acceleration is rather

calculated but, as it can be seen, it comes along with a lot of noise content. For the non-zero acceleration a rattle can be identified in contrast to the whine seen in the second part of the simulation. This makes sense as rattle is associated with varying loads, in this scenario likely caused by the clearance existing in the gear mesh that also generates backlash and an uneven transmission motion as velocity keeps increasing. Once the gears do not accelerate anymore, the noise becomes periodic and its frequency is higher because the periodic perturbances are now dominated by the manufacturing and assembling imperfections of the drive train that tend to increase the transmission error (see chapter 2.1.3).

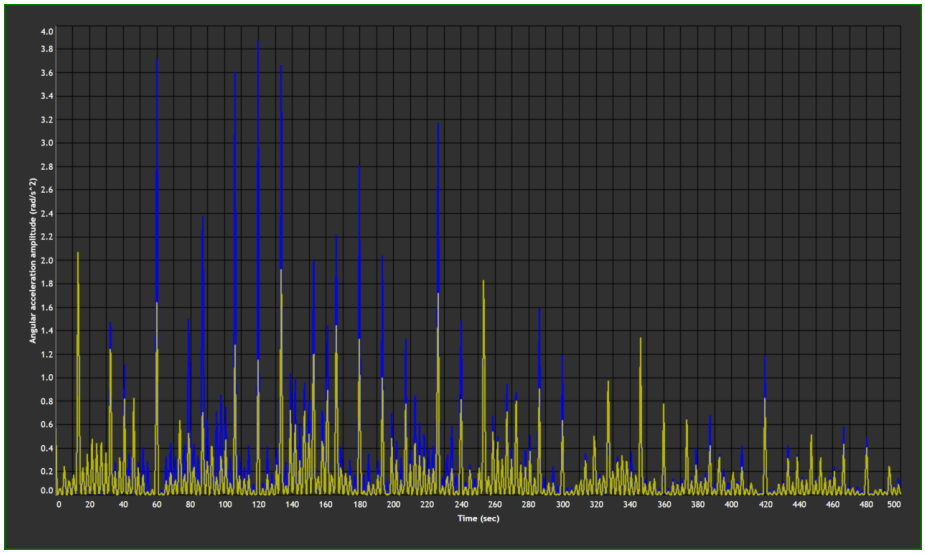

Figure 31: Frequency spectrum (FFT) of the angular acceleration (up to 500 Hz). Blue: planetary gear, yellow: drive sun gear

In the frequency domain analysis, the FFT of the whine noise is shown in figure 31. Both accelerations shows exactly the same frequency content for the two gears, fact that could confirm that the origin of this effect is the transmission error. The difference in amplitude should be a consequence of the different acceleration values experimented by each gear. Again, the shaft frequencies can be identified but they do not have the highest peaks. The frequency of 13 Hz is highlighted this time as well, along with multiples of the idler shaft frequency (i.e. 120 Hz and 180 Hz). Reckoning that the planetary gear is actually coupled with two gears can explain why its FFT curve has 120 Hz as the main frequency: a result of experimenting imperfect meshing twice per rotation.

Lastly, the STFTs of Figures 32 and 33 show, on their right side, a steady behaviour that complies with the frequency spectrum of the FFTs. On the left side, the possible rattle impact from Figures 23 and 24 makes an appearance again, and this time the plot also shows a second effect of the same nature (but with less intensity) at around 1.2 seconds. Just like with the frequency

amplitudes, all the phenomena seen in the STFT of the drive gear is similar in looking to the one of the idler but weaker in magnitude.

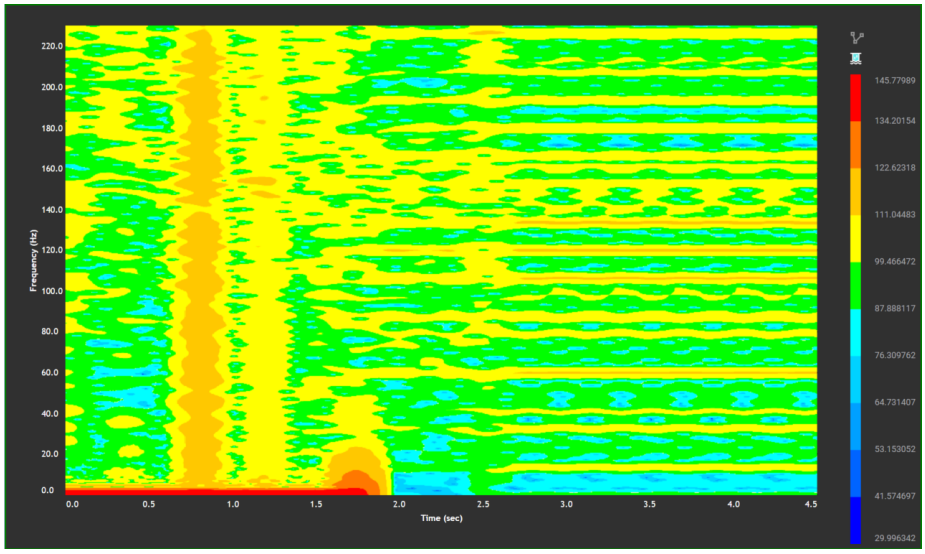

Figure 32: Colormap (STFT) plot of the angular acceleration of the planetary gear. Amplitude values shown in decibel scale.

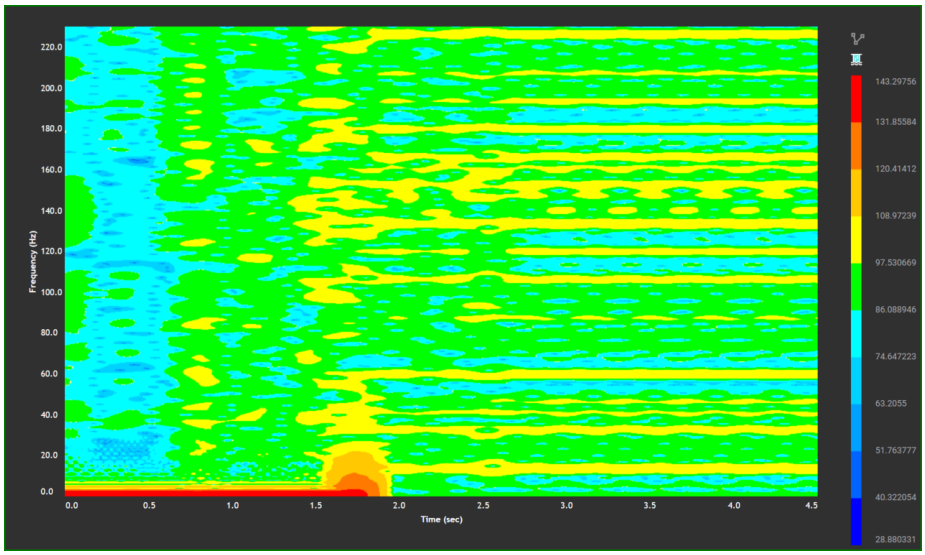

Figure 33: Colormap (STFT) plot of the angular acceleration of the drive sun gear. Amplitude values shown in decibel scale.

6.2 Dynamics

The dynamic analysis of the model is focused on the inspection of the physical causes that derive in unexpected effects in the system due to a gear-gear interaction, namely the mesh coupling of the (drive) sun - planetary and planetary - (driven) sun gear pairs, from now on also known as gear set 1 and gear set 2, respectively. For this purpose, force and torque simulated curves are shown and discussed, since they represent an alternate way to inspect the drive train vibrational behaviour. The transmission error resulting data will help to provide explanation to short-time disturbances and, finally, the misalignment effect between shafts is also briefly commented.

6.2.1 Forces

The verification of the gear forces helps not only to verify that the loading conditions given the input power are properly reproduced in the simulation but to serve, in some sense, as a vibration analysis method. For a proper study of vibrations, the common practice is to measure accelerations in a non-rotating component, for example, the housing of a gearbox. Unfortunately, for the proposed model all system elements are either rotating (i.e. gears) or fully constrained in a position in space (i.e. shaft's centre of rotation), so there is no ideal location to put a marker. The markers that allowed the measurements at the sun and planetary gears in chapter 6.1.1 could facilitate a first approach to analyse vibrations, nevertheless at the end the clearly dominant influence of the circular movement creates some bias that might not allow a proper distinction between vibration and kinematic motion signals. While it is not clear if (and how) forces are measured (through the use of markers) or calculated (based on the power/torque input data) in the Ansys Motion simulation, it is plausible to assume that they are in some way related to the local acceleration at the tooth engagement along the pressure line. Because these forces take place in a non-rotating location that is not completely constrained to its position in space (if a gear couple vibrate, their exact meshing location vibrates with them), there is the possibility that the resulting signals behave in a similar way to a marker placed in a gearbox housing.

Tangential and radial In Figure 34 the radial and tangential forces of the first gear set are shown. First thing to notice are the strong perturbances at specific instants of time in both curves (one even occurs at the same time as the perturbances observed in subchapters 6.1.1 and 6.1.2). The diagram also depicts a slight increment in the force values when the simulation has already passed the two seconds mark. Taking a closer look, this small increment lets the function to get closer to its theoretical value.

Because the curves behave in a periodic manner during the steady state phase, it is possible to make a frequency domain analysis about them (Figure 35). Naturally, the amplitudes of the tangential force are of higher magnitude than of the radial but, in general, the harmonic content is the same, so their

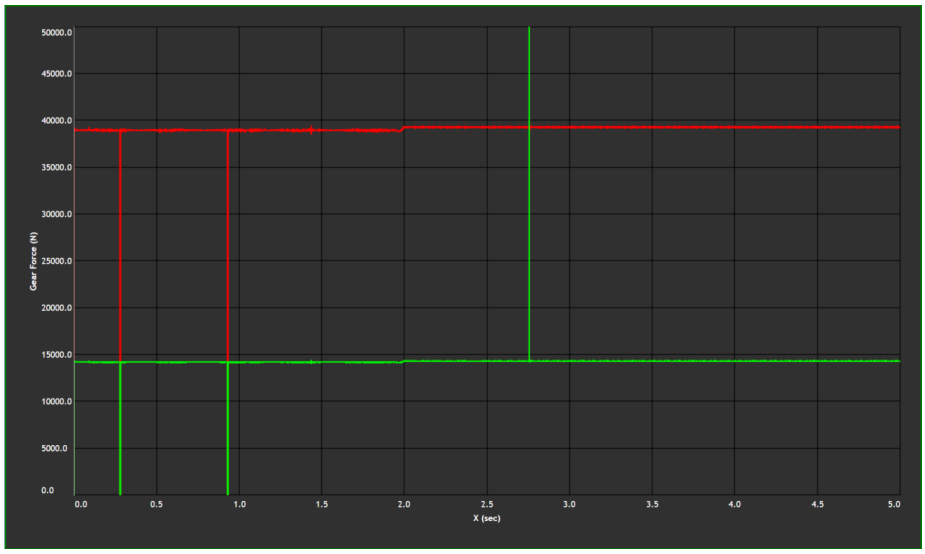

Figure 34: Variation of the tangential and radial forces at the gear set 1 over time. Red: tangential force F_y, green: radial force F_z

periodic behaviour can be assumed to be the equivalent. It is also interesting to notice that this spectra is very similar to the one of Figure 31, even when the latter is taken from angular accelerations.

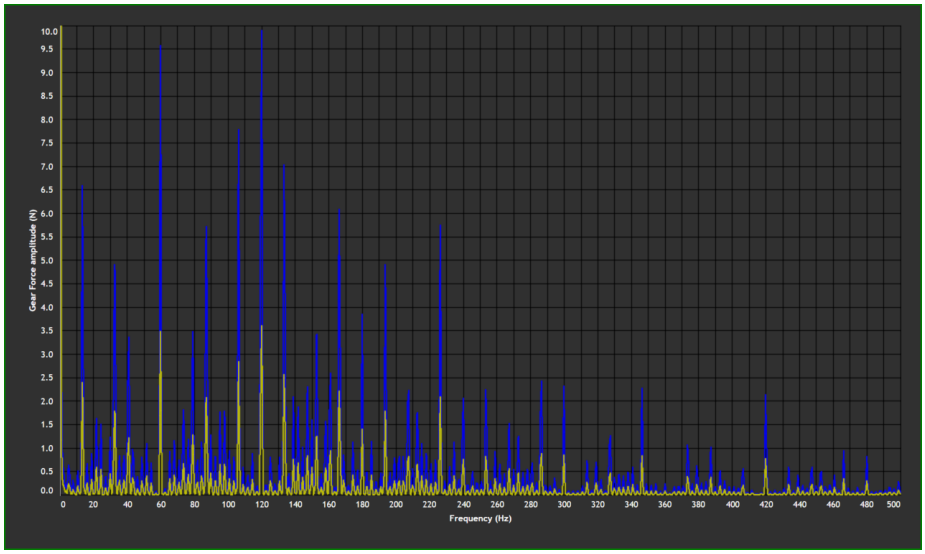

Figure 35: Frequency spectrum (FFT) of the tangential and radial forces at the gear set 1 (up to 500 Hz). Blue: tangential force F_y, yellow: radial force F_z.

The STFT plot of the tangential force (Figure 36) summarizes the behaviour observed in the previous figures. The sudden perturbances can be seen at the expected times and the frequency content appears as well, where 60 Hz and 120 Hz are the most dominant frequencies. From the transient response at the diagram's left side a rattle noise pattern can also be seen between the disturbance vertical lines.

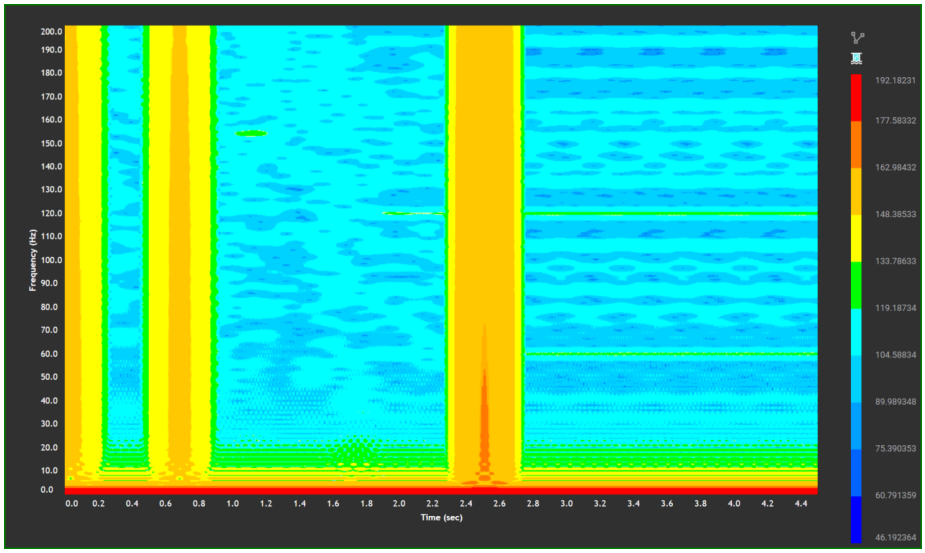

Figure 36: Colormap (STFT) plot of the tangential force at the gear set 1. Amplitude values shown in decibel scale.

Axial It is normal to expect that the axial force does not provide meaningful information when inspecting the dynamics of the drive train but one must have in mind that some dominant vibration modes occur precisely in this direction. [30] [31] Since this force is not measured at a specific marker but probably in the same coordinate system and origin as the tangential and radial forces (somewhere along the pressure line), any vibration in the x direction should be detected. Figures 37 to 40 prove this as they illustrate curves that oscillate periodically around zero. Specifically, they describe the tangential force measured at gear sets 1 and 2, that means, at both gear meshing contact points: drive-idler and idler-driven pairs.

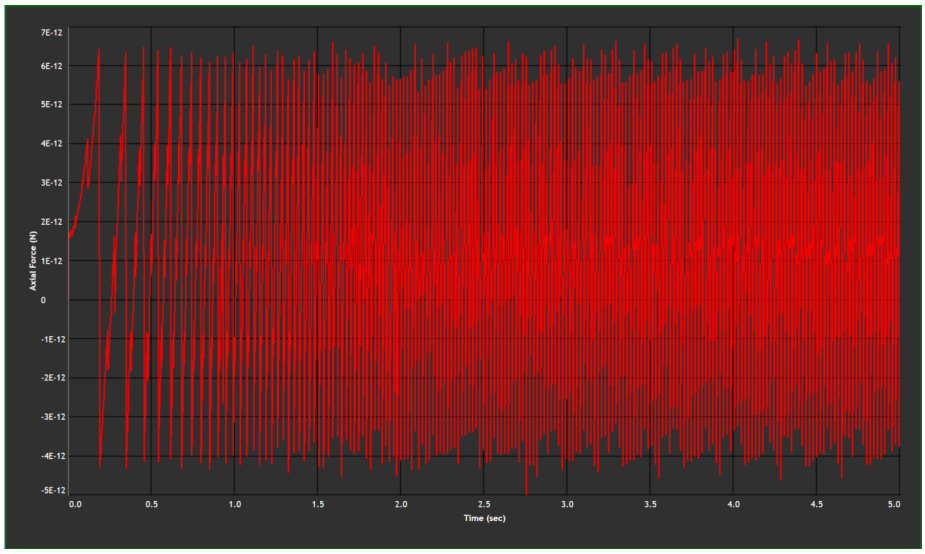

Figure 37: Variation of the axial force F_x at the gear set 1 over time.

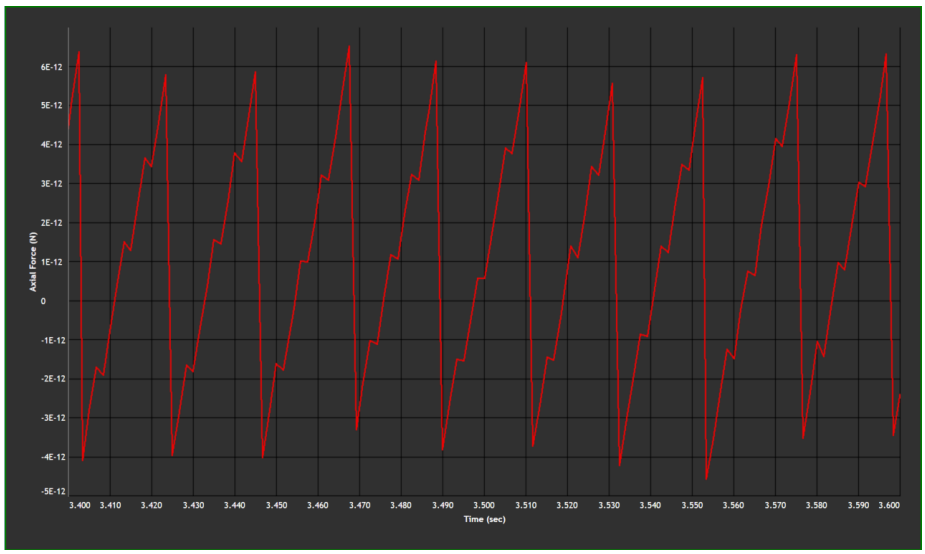

Figure 38: Variation of the axial force F_x at the gear set 1 over time (3.4 to 3.6 seconds).

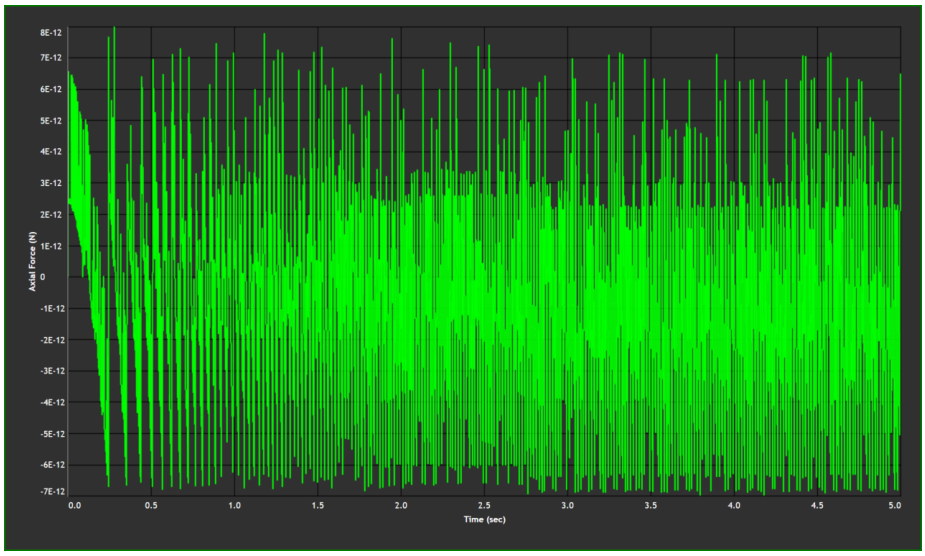

Figure 39: Variation of the axial force F_x at the gear set 2 over time.

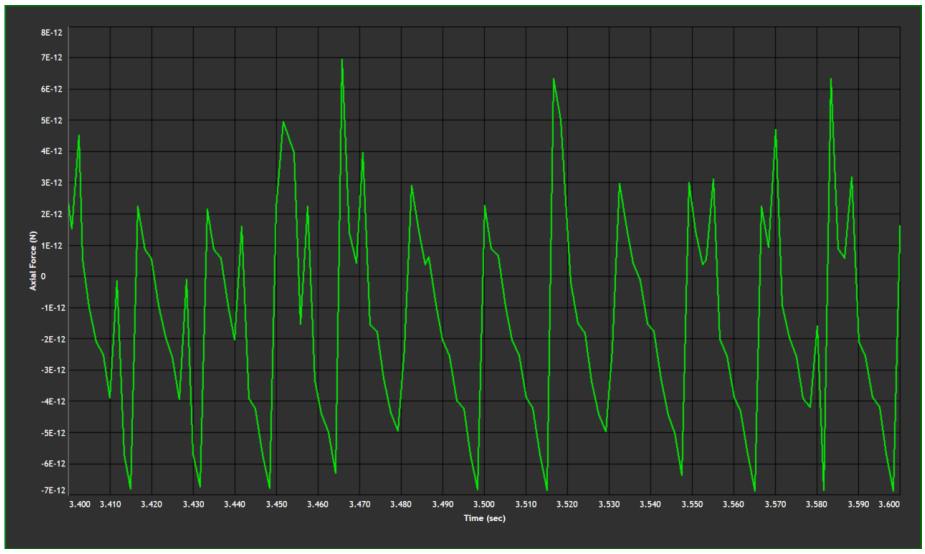

Figure 40: Variation of the axial force F_x at the gear set 12 over time (3.4 to 3.6 seconds).

Should the harmonic content of these signals be investigated through the FFT of Figure 41, it can be seen that the gear angular frequencies and their multiples have exclusive influence on the detected vibration. As seen in subchapter 2.1.3, this kind of behaviour is common for shaft misalignments, so the topic

will be brought back again later (see chapter **??**).

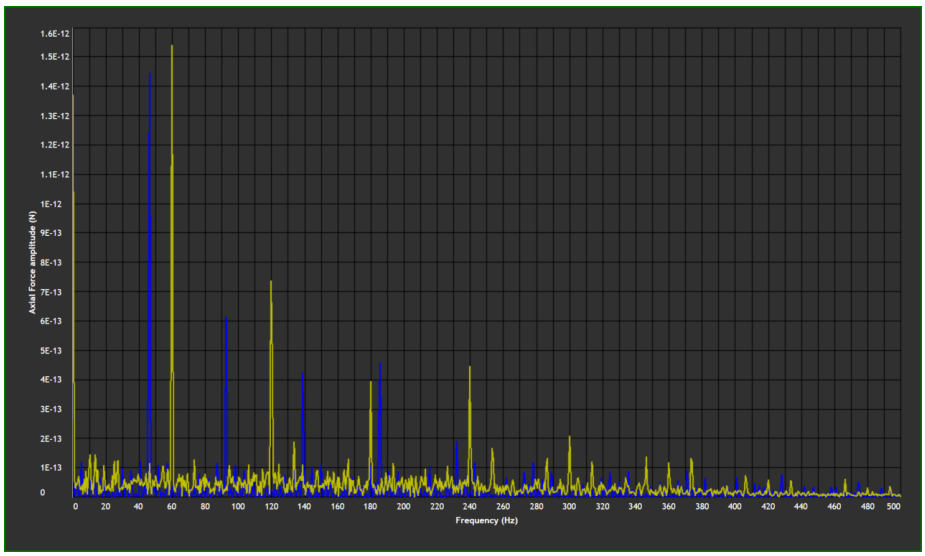

Figure 41: Frequency spectrum (FFT) of the axial force (up to 500 Hz). Blue: gear set 1, yellow: gear set 2

In the respective STFTs (Figures 42 and 43), it is visible how the frequencies evolve linearly as time increases until they reach a final constant value. That linear increase is the normally observed phenomena when employing the order tracking method (see chapter 2.2), which plots the RPM against frequency. Since the shaft frequency is proportional to the angular velocity and the system should not suffer of any unexpected disturbance, these results are probably one of the most accurate so far.

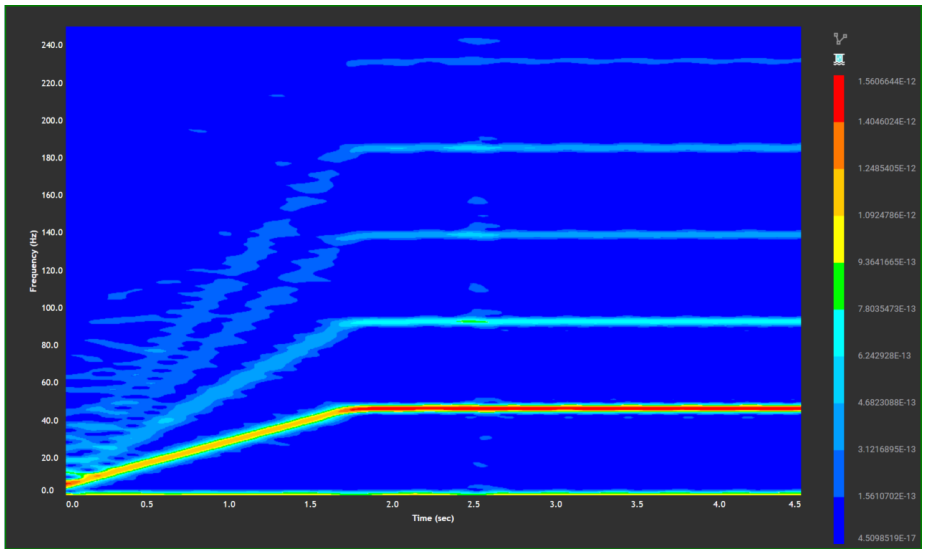

Figure 42: Colormap (STFT) plot of the axial force at the gear set 1.

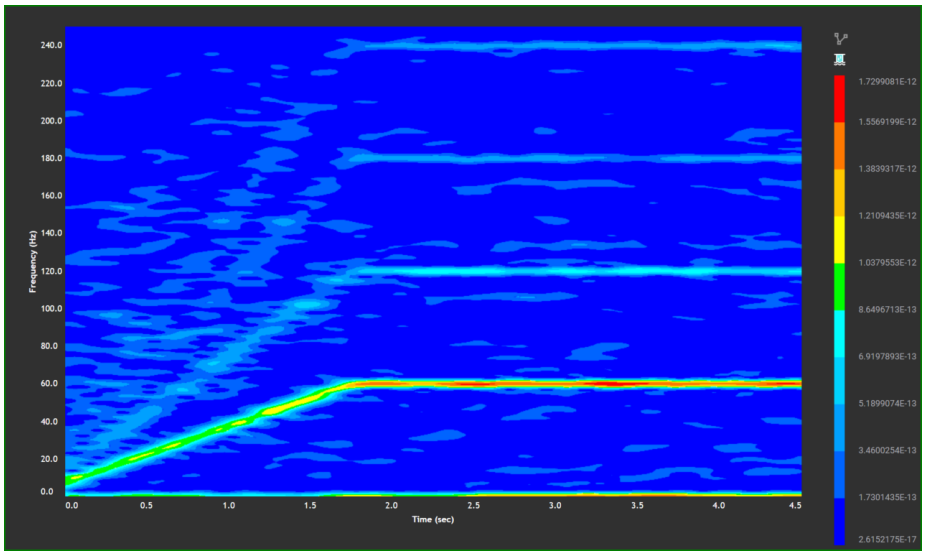

Figure 43: Colormap (STFT) plot of the axial force at the gear set 2.

Moreover, if a decibel scale is used for the colormaps (Figures 44 and 45), rattle patterns can be also seen, meaning that the transmission error also plays a role here.

Up to this point the gear mesh frequency has not been discussed. The reason for this is that it has not been detected in any of the simulation signals. As

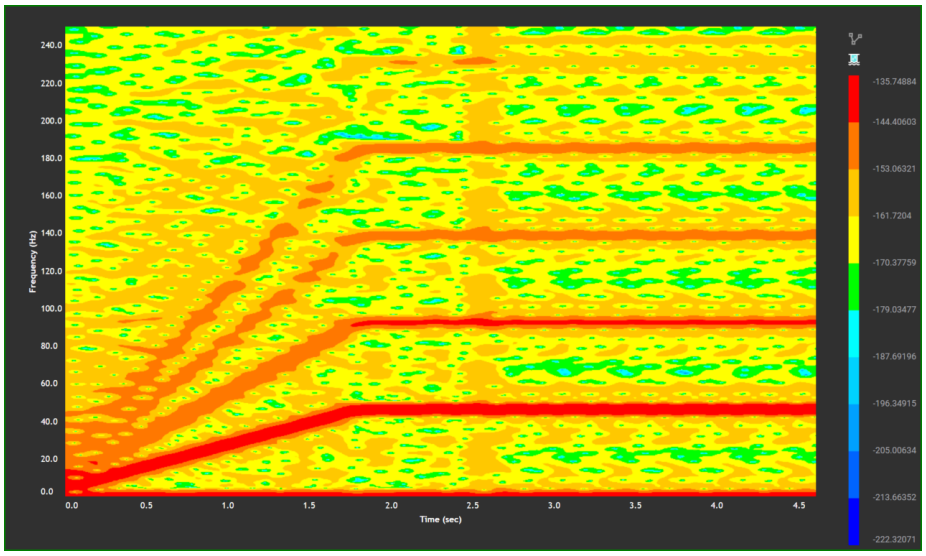

Figure 44: Colormap (STFT) plot of the axial force at the gear set 1. Amplitude values shown in decibel scale.

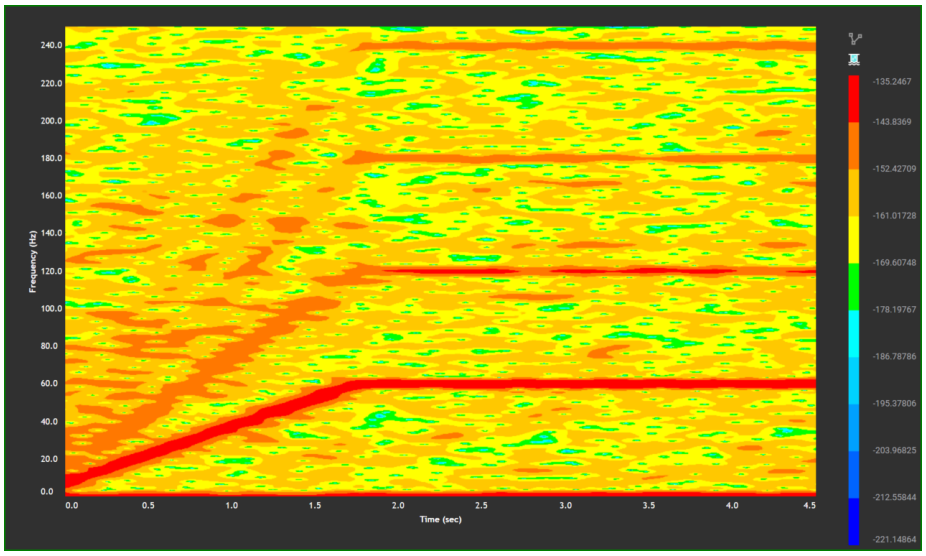

Figure 45: Colormap (STFT) plot of the axial force at the gear set 2. Amplitude values shown in decibel scale.

defined in chapter 5.4, that is quite unlikely to happen (or actually impossible) because the sample rate is lower than the objective frequency. In Figure 46 we can see the same FFT as in Figure 46 but in the decibel scale. Looking at

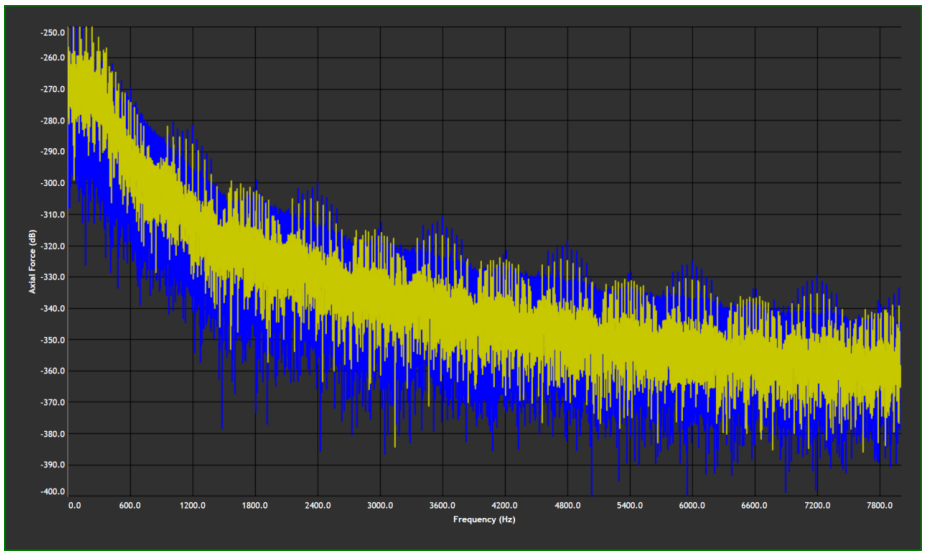

Figure 46: Frequency spectrum (FFT) of the axial force (up to 8100 Hz). Blue: gear set 1, yellow: gear set 2. Amplitude values shown in decibel scale.

the point where the GMF should be (3060 Hz), not even a slightly higher peak can be seen. But we do see that peak amplitude patterns are repeated over the spectrum, specifically every 1200 Hz. Along with these observed decaying peaks some sidebands also appear; they are just multiples of the shaft frequencies and this is true for both gear sets. It is yet unclear why this effect happens but, if instead of 1200 Hz, the frequency repeated were a multiple of the GMF, this could be a symptom of pitch diameter wearing or even tooth faults. This type of results strengthens the need of setting up an adequate number of output steps to have a proper sampling frequency and avoid important misinterpretations of the results.

6.2.2 Torques

Figure 47 shows the variation of the torque on the gear set. Both the graphs have certain disturbance in the form of sudden and distinct peaks at different times during the simulation. Some of the peaks in torque graphs (0.3s and 0.9s) correspond to the same peaks that were found in the peaks in tangential force (Figure 34). The spike in torque of sun gear at around 2.7s can be attributed to the sudden spike in radial force between the gear sets. The spikes are noticed on the planetary gear are caused because of the presence of backlash between each of the gears. The planetary gear has more spikes in its torque curve because the gear is in contact with two gears and has to deal with the backlash and transmission errors in both the gear pairs. The slight increase in forces discussed in section 6.2.1 can be seen as increase in torque in planetary gear and decrease

in torque in the sun gear. It implies that this was caused by a re-adjustment of the point of contact between the gear pair when the angular acceleration is stabilizes.

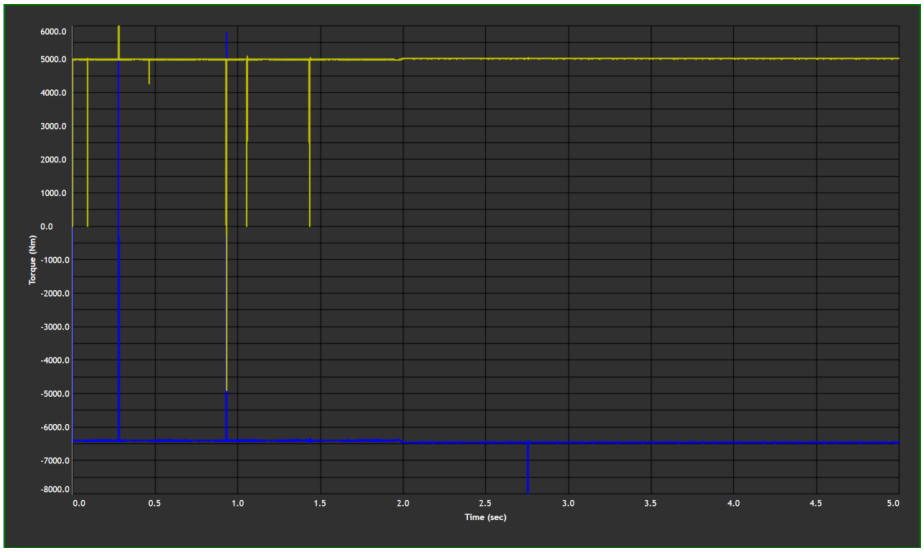

Figure 47: Variation of the Torque on the gear set over time. Blue: sun, yellow: planetary.

6.2.3 Transmission Error (TE)

The angular transmission error of the both the gear sets is shown in the Figure 48. Overall, the TE can be divided into two different phases that is clearly split along the acceleration periods of the gear. The sudden spike in TE can be seen at the same time as torque spikes of the planetary gear in figure 47. Each of the torque spikes can be attributed transmission error spikes. The remaining acceleration period can be explained by the rattle present in gear sets. The period with constant velocity (after 2.0s) can been to have a consistent and uniform TE corresponding to the whine in both the gears. The first gear set however has a deflection during this period at the time of 2.75s which can be attributed to the radial force and torque spike found in the sun gear. The remaining period with constant velocity shows a harmonic content of the whine which is consistent for both the gear sets as shown in Figure 49.

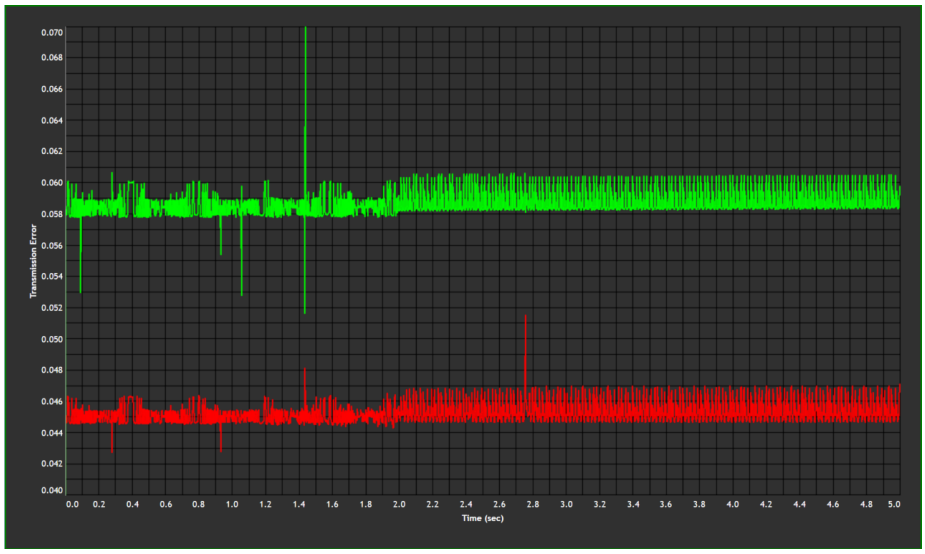

Figure 48: Variation of the Angular TE on the gear set over time. Red: gear set 1, green: gear set 2.

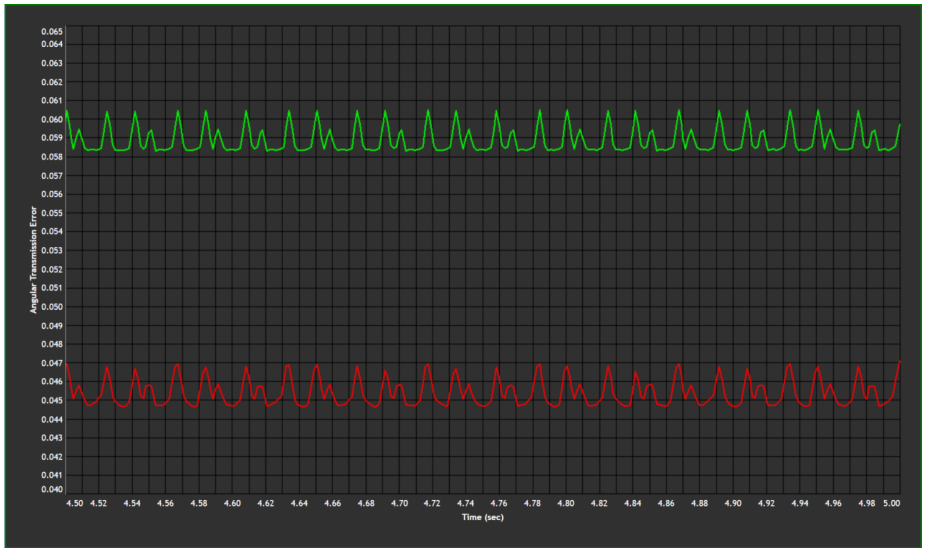

Figure 49: Variation of the Angular TE of the two gear sets over time (4.48 to 5.00 seconds).

In the frequency domain analysis, the FFT of the Angular TE is shown in the Figure 50. Both the gear sets show the exact same frequency domains which clearly imply that the sources for TE in both the cases are the same. Biggest

spikes in amplitude are noted at 47Hz, 73 Hz and 120Hz which are similar to the spikes found in the FFT of the planet's linear acceleration magnitude in Figure 21

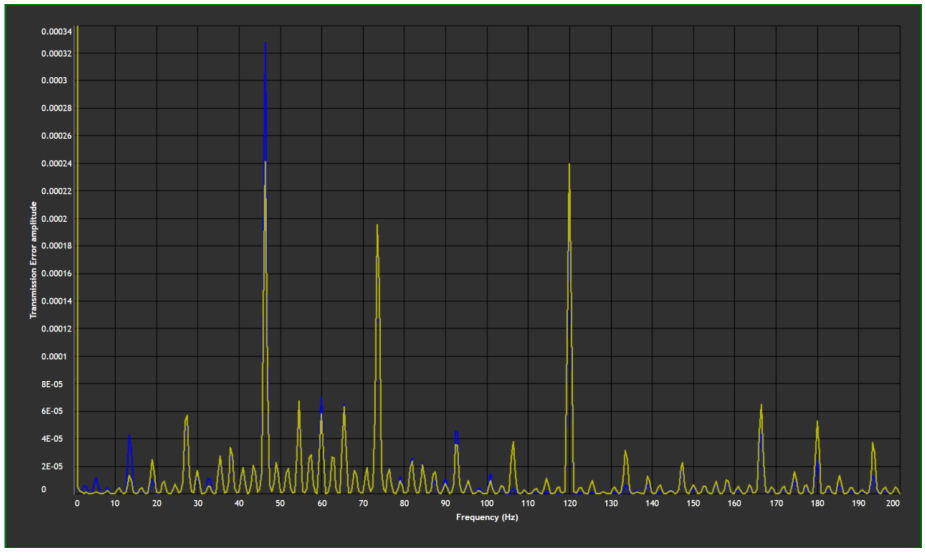

Figure 50: Frequency spectrum (FFT) of the Angular TE(up to 200hz). Blue: gear set 1, yellow: gear set 2.

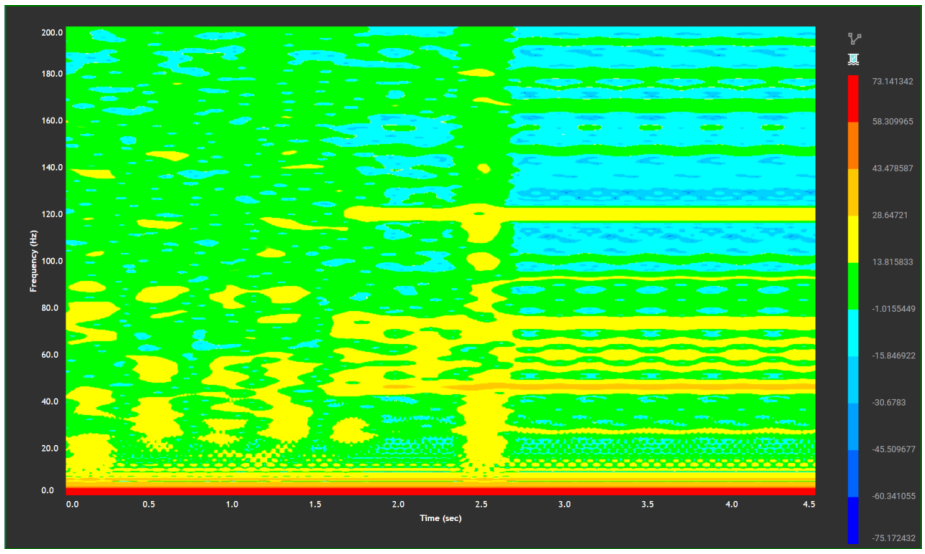

Figure 51: Colormap (STFT) plot of the Angular TE of the gear set 1- version 1. Amplitude values shown in decibel scale.

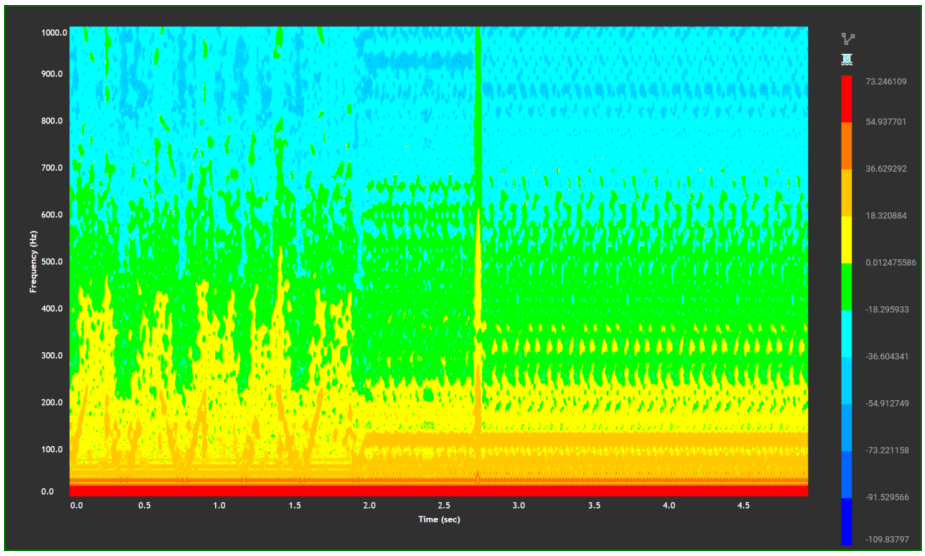

Figure 52: Colormap (STFT) plot of the Angular TE of the gear set 1- version 2. Amplitude values shown in decibel scale.

In the different versions of the following colormaps we vary the time slice (see Section 5.6) to observe different effects. Figure 51 and 52 are for gear set 1 and Figure 53 and 54 are for gear set 2. In version 1, the harmonic content at steady state is clearly distinguished for both the cases. However, gear set 1 shows a clear spike at 2.75s. This spike is also noticed in the Angular TE of gear set 1 in Figure 48. In version 2, we see some strange diagonals that could be rattle during the transient phase.

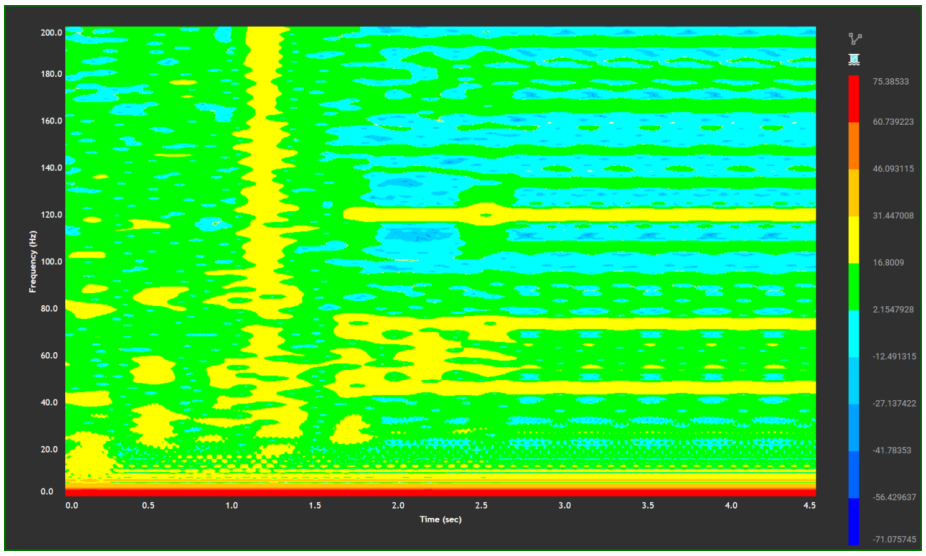

Figure 53: Colormap (STFT) plot of the Angular TE of the gear set 2- version 1. Amplitude values shown in decibel scale.

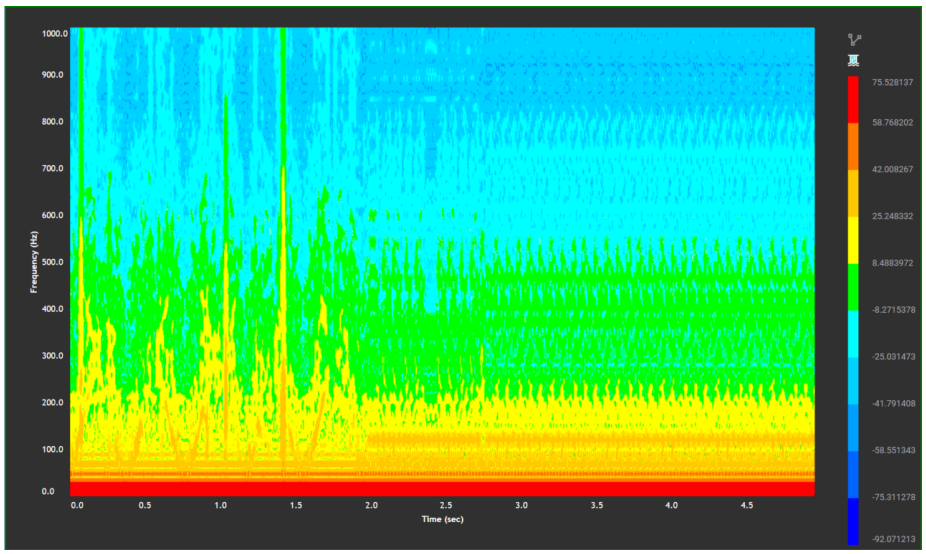

Figure 54: Colormap (STFT) plot of the Angular TE of the gear set 2- version 2. Amplitude values shown in decibel scale.

6.2.4 Misalignment

The Misalignment of the both the gear sets is shown in the Figure 48. Any misalignment present in the gears implies that natural rotation of the gears becomes more difficult which intern results in higher vibration and in some cases variable acceleration. Due to the motions of the gears, small amounts of variable misalignments creep up in the simulation in addition to the existing misalignment. In the acceleration phase, the spikes appear at similar time when compared angular TE and angular acceleration which indicates that the quantities are related. It must be noted that the angular acceleration spike for in constant velocity phase for planetary gear at 2.75s (Figure 29) is not present in misalignment.

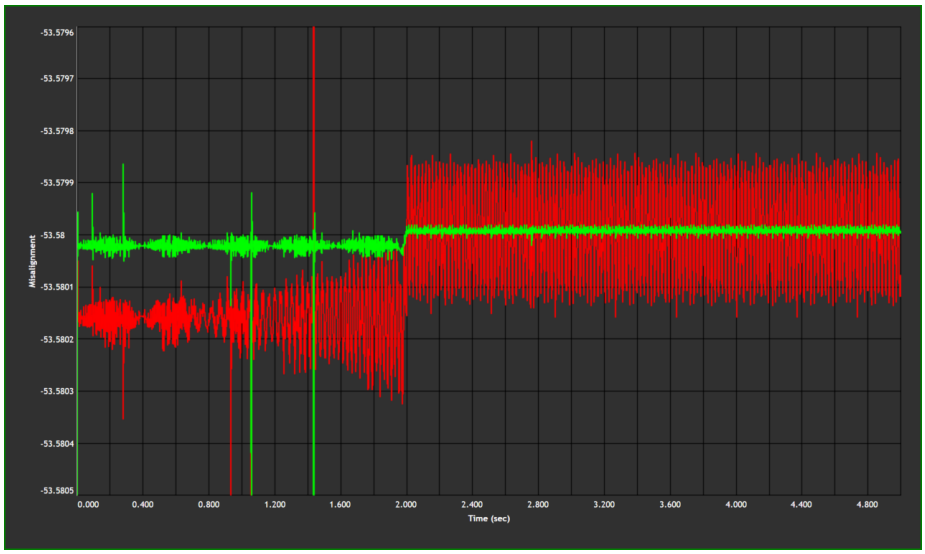

Figure 55: Variation of the Misalignment on the gear set over time. Red: gear set 1, green: gear set 2.

In the second phase of the simulation, the misalignment becomes harmonic for both the gear sets. This can be easily seen in the Figure 56. It should be noted that the misalignment variation in the gears is much smaller in gear set 2. The FFT analysis for misalignment, shown in figure 57 and **??**, shows the reason for this difference. Gear set 1 has a peak misalignment that is repeated at the frequency of rotation of the sun gear(47Hz). Other peaks are miniscule in comparison. The STFT of the first gear set in figure 58 shows a distinct shade in at around 47hz.

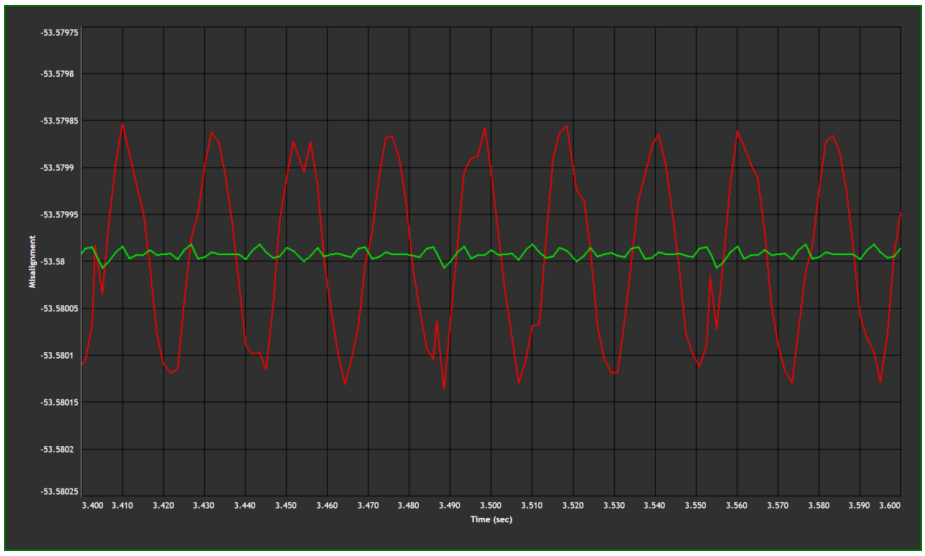

Figure 56: Variation of the Misalignment of the two gear sets over time (3.4 to 3.6 seconds). Red: gear set 1, green: gear set 2.

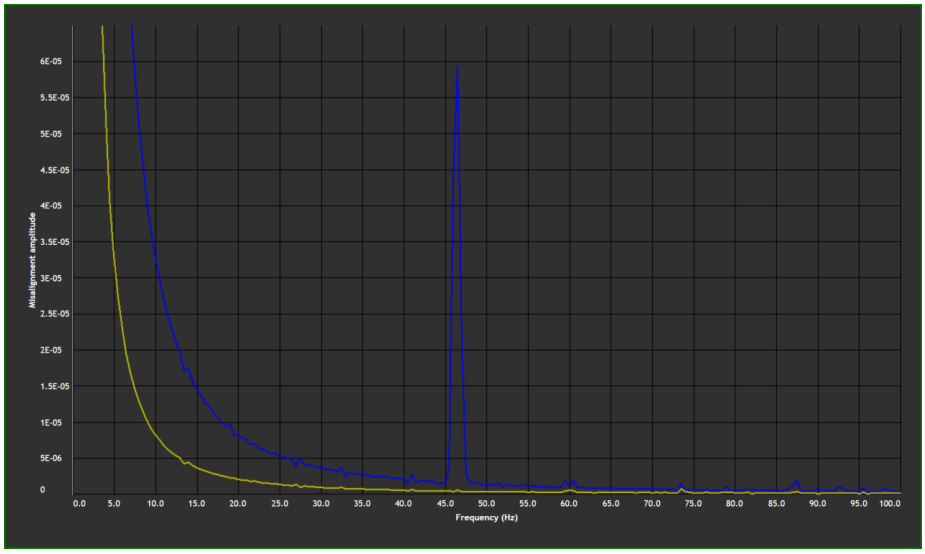

Figure 57: Frequency spectrum (FFT) of the Misalignment(up to 100hz). Blue: gear set 1, yellow: gear set 2.

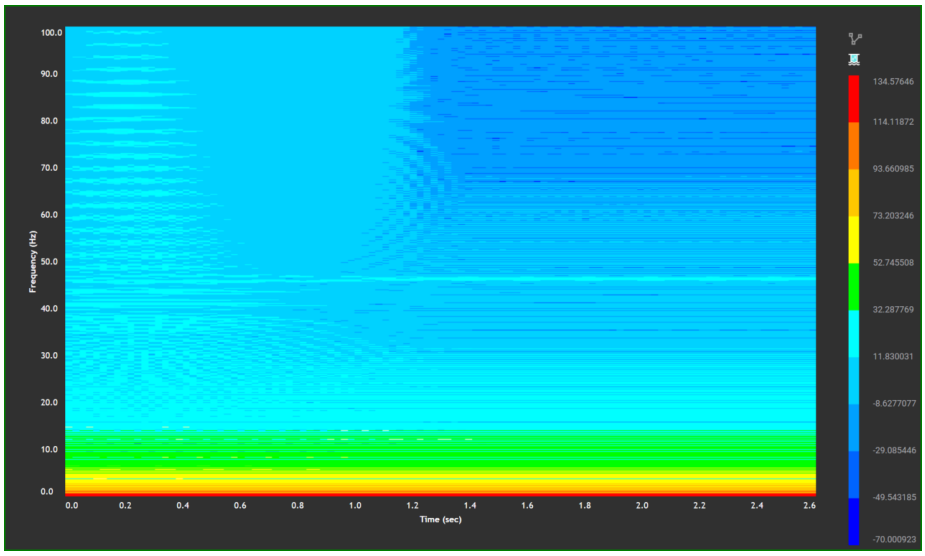

Figure 58: Colormap (STFT) plot of the Misalignment of the gear set, gear set 1.

6.3 Drive train data

6.3.1 Dynamic Peak-to-Peak Transmission Error (PPTE)

For an explanation of the expected results, the pre- and post-processor manuals can be consulted. This concept is explained there and also misalignment. This could also be found in the drive train guide ppt.

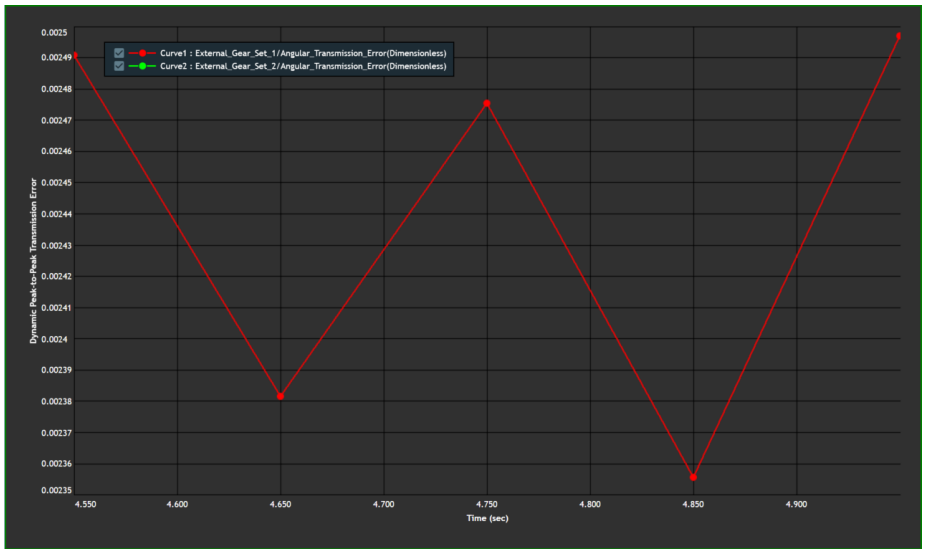

Figure 59: PPTE, gear set 1.

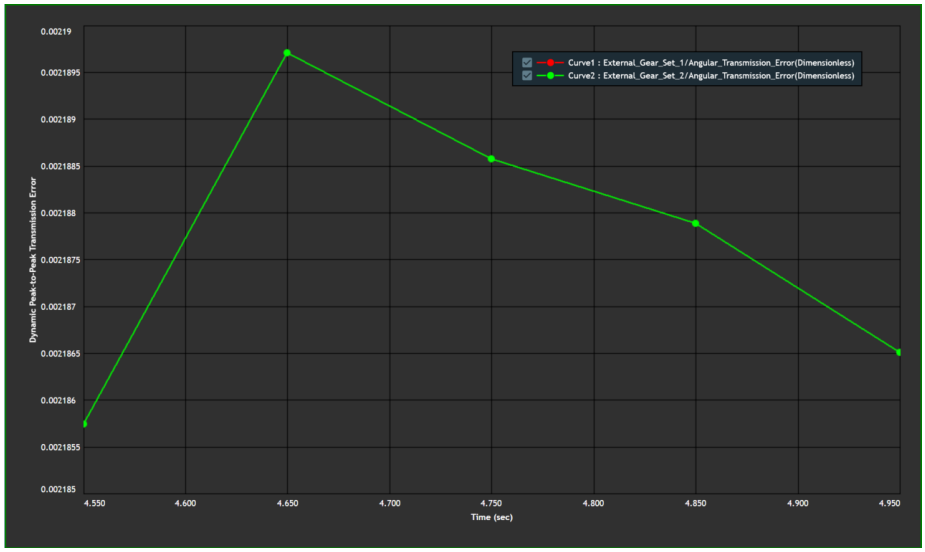

Figure 60: PPTE, gear set 2.

6.3.2 Tooth Contact Pressure (TCP)

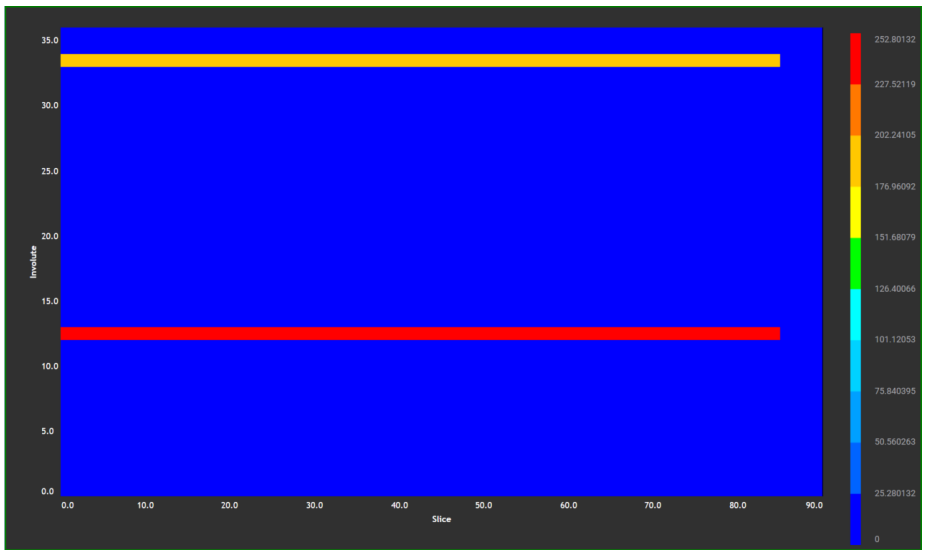

Figure 61: Tooth Contact Pressure

7 Conclusions

Key ideas:

- Discussion of kinematics
- Discussion of dynamics
- Relevance of both fields in relation to vibration analysis. Which set of results is more relevant for this? What were those results and what do they mean?
- Shaft frequencies were detected but GMF no
- Transmission error had influence on some graphs as noticed in the whine noise
- The rattle noise should be better investigated and the sudden perturbances too
- No resonances apparent
- Assessment of Ansys Motion: Good for kinematic analysis, bad for vibration analysis. STFT functionalities don't operate as desired. An order tracking analysis (RPM vs f) is better for this kind of task but is not available in the software. TCP does not work. Analysis could be better if a whole assembly is tested (+bearings,+housing,+shafts as flexible entities).

8 References

[1] C. Glinsky, "Rotational Mechanics / Kinematics," *Drivetrain Hub LLC*, 2020. [Online]. Available: https://drivetrainhub.com/notebooks/fundamentals/rotational_mechanics/Chapter%202%20-%20Kinematics.html

[2] S. Radev, "Einfluss von Flankenkorrekturen auf das Anregungsverhalten gerad- und schrägverzahnter Stirnradpaarungen," Dissertation, Technische Universität München, München, 2007.

[3] M. K. Heider, "Schwingungsverhalten von Zahnradgetrieben," Dissertation, Technische Universität München, München, 2012.

[4] B. Neubauer, "Lastverteilung und Anregungsverhalten in Planetengetriebesystemen," Dissertation, Technische Universität München, München, 2016.

[5] R. Shao, P. Jia, and F. Dong, "Dynamic characteristics of cracked gear and three-dimensional crack propagation analysis," *Proceedings of the Institution of Mechanical Engineers, Part C: Journal of Mechanical Engineering Science*, vol. 227, no. 6, pp. 1341–1361, 2013.

[6] T. Berninger, "Experimental Vibration Analysis," Lecture Script - Version 1.0 Winter Semester 2019, Technical University of Munich, München, 2020.

[7] Siemens AG, "Fundamentals of DSP - Introduction to Digital Signal Processing," 2017.

[8] Siemens PLM Software, "The Metric for Gearbox NVH Quality," *Transmission Error*, 2014.

[9] M. Cerna and A. F. Harvey, "The fundamentals of FFT-based signal analysis and measurement," Application Note 041, National Instruments, Tech. Rep., 2000.

[10] A. Brandt, T. Lago, K. Ahlin, and J. Tuma, "Main principles and limitations of current order tracking methods," *Sound and Vibration*, vol. 39, no. 3, pp. 19–22, 2005.

[11] M. Åkerblom, "Gear Geometry for Reduced and Robust Transmission Error and Gearbox Noise, Report, Maskinkonstruktion," *Machine Design, Trita-MMK, ISSN*, vol. 14001179, 2008.

[12] M. Benatar, M. Handschuh, A. Kahraman, and D. Talbot, "Static and Dynamic Transmission Error Measurements of Helical Gear Pairs With Various Tooth Modifications," *Journal of Mechanical Design*, vol. 141, no. 10, 05 2019, 103301. [Online]. Available: https://doi.org/10.1115/1.4043586

[13] Ansys, Inc., "ANSYS Motion Drivetrain Technical Document Updated for Mechanical," 2021.

[14] A. Fernandez, "Vibration analysis learning," *Power-MI*, 2022. [Online]. Available: https://power-mi.com/content/vibration-analysis-learning

[15] P. Sopcik and D. O'Sullivan, "How Sensor Performance Enables Condition-Based Monitoring Solutions," *5 Making Sense of Sounds, or How AI Can Boost Your Machines' Uptime*, p. 45, 2019.

[16] Ansys, Inc., "Ansys Motion: Simulation of a complete assembly of E-powertrain system," 2021.

[17] C. Scheffer and P. Girdhar, *Practical machinery vibration analysis and predictive maintenance*. Elsevier, 2004.

[18] The MathWorks, Inc., "Vibration Analysis of Rotating Machinery," 2022. [Online]. Available: https://de.mathworks.com/help/signal/ug/vibration-analysis-of-rotating-machinery.html

[19] R. Tharmakulasingam, "Transmission error in spur gears: Static and dynamic finite-element modeling and design optimization," Ph.D. dissertation, Brunel University School of Engineering and Design PhD Theses, 2010.

[20] V. Philippe, "On the modelling of spur and helical gear dynamic behaviour," *Mechanical engineering*, 2012.

[21] R. B. R. Sweeney, P. J., "Gear transmission error measurement using phase demodulation," *Journal of Mechanical Engineering Science*, 1996.

[22] R. B. Randall, Z. Y. Chin, W. Smith, and P. Borghesani, "Measurement and use of transmission error for diagnostics of gears," in *Surveillance, Vishno and AVE conferences*, 2019.

[23] R. Hjelm, A. Ahadi, and J. Wahlström, "Gear tolerancing for simultaneous optimization of transmission error and contact pressure," *Results in Engineering*, vol. 9, p. 100195, 2021. [Online]. Available: https://www.sciencedirect.com/science/article/pii/S2590123020301031

[24] R. Parker and J. Lin, "Modeling, modal properties, and mesh stiffness variation instabilities of planetary gears. prepared for nasa," NASA/CR-2001-210939, Tech. Rep., 2001.

[25] P. Kelly and M. Menday, "Various forms of transmission rattle in automotive powertrains," in *Tribology and Dynamics of Engine and Powertrain*. Elsevier, 2010, pp. 839–856.

[26] G. Dalpiaz, A. Rivola, and R. Rubini, "Effectiveness and sensitivity of vibration processing techniques for local fault detection in gears," *Mechanical systems and signal processing*, vol. 14, no. 3, pp. 387–412, 2000.

[27] Z. Neusser, M. Sopouch, T. Schaffner, and H.-H. Priebsch, "Multi-body dynamics based gear mesh models for prediction of gear dynamics and transmission error," *SAE Technical Paper*, pp. 01–0897, 2010.

[28] *Assessment of the Vibration Excitation and Optimization of Cylindrical Gears*, ser. International Design Engineering Technical Conferences and Computers and Information in Engineering Conference, vol. Volume 8: 11th International Power Transmission and Gearing Conference; 13th International Conference on Advanced Vehicle and Tire Technologies, 08 2011. [Online]. Available: https://doi.org/10.1115/DETC2011-47443

[29] A. Bliznyuk, I. Dadon, R. Klein, and J. Bortman, "Gear diagnostics–fault type characteristics," in *Annual Conference of the PHM Society*, vol. 6, no. 1, 2014.

[30] H. C. Pusey and S. C. Pusey, "Current Practices and Trends in Mechanical Failure Prevention. Proceedings of the Meeting of the Mechanical Failures Prevention Group (44th) Held in Virginia Beach, Virginia 3-5 April 1990," VIBRATION INST WILLOWBROOK IL, Tech. Rep., 1990.

[31] E. Swanson, C. D. Powell, and S. Weissman, "A practical review of rotating machinery critical speeds and modes," *Sound and vibration*, vol. 39, no. 5, pp. 16–17, 2005.